Angular correlations and the isotropic-nematic phase transition in suspensions of tobacco mosaic virus

Seth Fraden* and Georg Maret
Hochfeld Magnetlabor, Max Planck Institut, Grenoble, France

D. L. D. Caspar
Rosenstiel Center for Basic Medical Sciences, Brandeis University, Waltham, Massachusetts 02254
(Received 19 April 1993)

The specific magnetic-field-induced birefringence is measured in aqueous suspensions composed of the charged rodlike particle tobacco mosaic virus (TMV) as a function of temperature, TMV concentration, ionic strength, and TMV polydispersity over the entire isotropic range. This quantity is proportional to the magnitude of the interparticle angular correlations at zero field. Theoretical expressions for the field-induced birefringence for both the mono- and polydisperse samples are derived based on extensions of the Onsager model [L. Onsager, Ann. N.Y. Acad. Sci. **51**, 627 (1949)] and compare well with experiment. In addition, the isotropic-nematic phase coexistence concentrations are measured as a function of ionic strength and temperature. The agreement between experiment and theory indicates that the TMV particles interact primarily through electrostatic repulsion and that attractive forces are negligible.

PACS number(s): 61.30.Gd, 61.25.Hq, 64.70.Md

I. INTRODUCTION

The phase behavior and macroscopic properties of condensed phases are determined by interparticle interactions, which generally have both repulsive and attractive components. The noble elements, such as liquid argon, serve as model experimental systems to explore properties of single-component fluids for which the interactions are dominated by steric repulsion, with attractive forces playing a secondary role [1]. However, for fluids composed of anisotropic molecules there are no analogs to noble gases. In particular, the interactions between molecules which form thermotropic liquid-crystalline phases, have both important repulsive and attractive components [2].

Here we study colloidal suspensions of tobacco mosaic virus (TMV), which consist of rigid rodlike particles interacting almost entirely through electrostatic repulsion [3]. Similarly to recent computer simulations of hard rods [4], TMV suspensions exhibit a rich phase behavior and observations of isotropic [5], nematic [6], smectic, and colloidal crystalline phases [7–9] have been reported. In this respect, the TMV system is unique in being the only experimental system of particles whose pair potential is dominated by repulsion to show the same phase behavior as thermotropic liquid crystals. As a consequence of the simplicity of the interparticle interactions, there is hope that simple molecular statistical-mechanical theories, such as extensions of the Onsager model for nematic liquid crystals [10] discussed in this paper, will quantitatively describe these model TMV systems.

In this paper, we measure concentrations of the coexisting isotropic and nematic phases in suspensions of both monodisperse and polydisperse suspensions of TMV as a function of ionic strength and temperature. We use the technique of magnetic birefringence to examine the growth of angular correlations between particles throughout the entire isotropic phase as the particle concentration is increased towards the isotropic-nematic phase transition at constant temperature. We show that these magnetic birefringence studies as a function of TMV concentration and temperature yield information about the mass average of the TMV particles in suspension, the excluded volume of the particles, and the number of particles in an angular correlation volume. Our measurements are in good agreement with a theoretical description based on the Onsager model, which assumes that TMV particles interact exclusively through electrostatic repulsion, and that the angular correlations, excluded volume, and phase coexistence concentrations are independent of temperature.

The remainder of the paper is organized as follows. Section II introduces the TMV particle and mentions previous studies of liquid-crystalline phase of TMV. Section III discusses the previous observations of magnetic birefringence of virus suspensions. Theoretical models are developed for magnetic-field-induced birefringence in the isotropic phase, for both monodisperse and polydisperse suspensions. Section IV describes the theory for the concentrations of the isotropic-nematic coexistence region. Section V describes the experimental apparatus and sample preparation. Section VI discusses the experimental results. First, results of monodisperse samples are presented. The temperature dependence of the magnetic birefringence and coexistence concentrations are discussed in Secs. VI A–VI D, the concentration dependence of the specific magnetic birefringence in Sec. VI E, determination of $\Delta\chi$ in Sec. VI F, the concentration dependence of angular correlations in Sec. VI G, and the concentration dependence of the coexistence region as a function of ionic strength in Sec. VI H. Next, experiments with TMV samples with length polydispersity are discussed. In Sec. VI I observation of aggregation of TMV in suspensions of low ionic strength is reported.

Magnetic birefringence data of polydisperse samples is presented in Sec. VI K, and Secs. VI L and VI M discuss the segregation of longer particles into the nematic phase of co-existing samples. Finally, in Sec. VII, we present our conclusions.

II. TOBACCO MOSAIC VIRUS

In a low-resolution electron micrograph tobacco mosaic virus appears as a rigid rod of dimensions 3000 Å in length by 180 Å in diameter. As a consequence of its shape anisotropy, TMV is also optically anisotropic with different indices of refraction along and perpendicular to its axis; we denote the birefringence of a suspension of perfectly aligned particles by Δn_{sat}. Correspondingly, a TMV molecule has different diamagnetic susceptibilities along and perpendicular to the rod axis, the difference of which is denoted by $\Delta\chi$. A suspension of these particles is isotropic at low concentrations, that is, the rod axes point in all directions with equal probability when averaged over the entire sample. However, locally there are angular correlations between neighboring rods and the correlation length increases with concentration. At volume fractions varying between 2% and 10% (depending on ionic strength) the suspension forms a nematic liquid crystal. This is a fluid where the rod axes preferentially point in the same direction and the angular correlation length is infinite. Onsager [10] developed a model for this phase transition of a suspension of anisotropic particles. He showed that it is driven only by the shape anisotropy of the particles and that attractive van der Waals forces are not necessary to produce an ordered phase. In this case, the system is athermal and temperature plays no role in the phase behavior. However, TMV is a polyelectrolyte and at *p*H7 is negatively charged with a linear charge density of 0.5–2 electrons/Å (e/Å) [11]. In Onsager's model this alters the effective diameter of the particle, which is determined by the repulsive potential between rods. Adding salt to the suspension screens the repulsion and alters the effective diameter, thus accounting for the ionic strength dependence of the coexistence concentrations.

Previous studies of liquid-crystalline phases of TMV

Shortly after TMV was first isolated from infected tobacco plants, it was recognized that concentrated, purified suspensions formed a nematic liquid-crystalline phase. Best [12] measured the coexistence concentrations in NaCl solutions. Detailed x-ray and optical microscopic studies of TMV suspensions as a function of TMV concentration, pH, and ionic strength were performed by Bernal and Fankuchen [13]. However, the samples used in these early studies were polydisperse. Nematic phases of monodisperse TMV were studied by Oster [7], who used light scattering to measure the excluded volume of TMV in the isotropic phase as a function of ionic strength. Viscoelastic constants of TMV were measured by Fraden *et al.* [14] who also studied reorientation instabilities [15,16]. The orientational distribution function of the nematic director was measured by Oldenbourg *et al.* [17] as a function of concentration. Zasadzinski *et al.* [18] used freeze fracture electron microscopy to visualize the molecular ordering of TMV suspensions. In a companion letter to this paper, Fraden *et al.* [6] reported the measurements of the isotropic-nematic coexistence concentrations as a function of ionic strength.

Phases with greater order than nematic have also been reported. TMV forms crystalline inclusions in the infected tobacco plants. These crystals have been studied with optical microscopy [19] and freeze-fracture electron microscopy [20]. In studies of the phase behavior of monodisperse TMV, Oster [7] observed an iridescent phase of TMV in suspensions in pure water at low ionic strength. The iridescence arose from the ordering of the TMV molecules into layers perpendicular to the TMV axis, a structure consistent with either the smectic-A or colloidal crystalline phases. In a light scattering study, Kreibig and Wetter [8] measured the concentration dependence of the layer spacing in polydomain samples, and noted a large variation in lattice spacing for different domains in the same sample. Fraden, Caspar, and Phillips [21] studied the same iridescent samples, but with x-ray scattering, and measured the interparticle separation of the particles within the planes. They observed crystalline order, demonstrating that the iridescent phase, in pure water, was a colloidal crystal. Similarly to the observations of Kreibig and Wetter, they observed a large variation in lattice constant for crystals in the same physical conditions. Subsequently, in a combined optical microscopy, light and x-ray scattering study, Wen, Meyer, and Caspar [9,22] identified different conditions under which TMV forms a smectic-A phase. A review of experimental results for other lyotropic systems has recently been presented by Vroege and Lekkerkerker [23].

III. MAGNETIC BIREFRINGENCE

Application of a magnetic field (H) to an isotropic suspension of number density c induces partial alignment of the particles and the suspension becomes macroscopically birefringent. The specific magnetic birefringence in the limit of zero applied field $\Delta n/cH^2$ of the suspension is proportional to the number of particles in a correlation volume. Photinos *et al.* [24] reported magnetic birefringence measurements of a TMV solution at concentrations far below the nematic phase transition. They observed

$$\frac{\Delta n}{cH^2} \sim (c^* - c)^{-1}(T - T^*)^{-1} \tag{1}$$

which is characteristic for pretransitional orientational correlations with T the temperature and c^* and T^* experimentally determined constants having values of $c^* = 107$ mg/ml and $T^* = 130$ K.

A. Thermotropics

Magnetic birefringence has been frequently used in phase-transition studies of thermotropic liquid crystals [25]. Thermotropics are single-component systems com-

posed of anisotropic organic molecules. They are relatively incompressible and the density varies little with temperature. In experiments with thermotropics the field induced birefringence in the isotropic phase is measured as a function of temperature. The birefringence (Δn) increases as the temperature of the isotropic phase is lowered and is well described by the mean-field formula

$$\Delta n/H^2 \propto (T-T^*)^{-1} . \quad (2)$$

The birefringence does not increase without bound as the temperature is lowered. At zero magnetic field, for a temperature T_n which is greater than T^*, a phase transition to the nematic phase occurs. T^* is a constant obtained by extrapolating the values of T to where Δn diverges, which is the temperature where the isotropic phase is absolutely unstable. In a phenomenological theory, such as the Maier-Saupe model, T^* is related to the potential of mean force acting on a molecule in the nematic phase, and thus indirectly related to the attractive interparticle pair potential [2,26]. An explanation of the increase of the birefringence is that angular correlations between the molecules grow as the nematic transition is approached. de Gennes [27] has proposed that the angular correlation length, ξ, is given by $\xi^2 \propto (T-T^*)^{-1}$. In contrast, a fluid of noninteracting particles will never have a nematic transition or equivalently $T^*=0$. Such a fluid has a magnetic susceptibility given by $\Delta n/H^2 \propto 1/T$. The ratio of susceptibility for the interacting case [Eq. (2)] to the noninteracting case at the temperature of the isotropic to nematic phase transition (T_n) is $T_n/(T_n-T^*)$. This ratio is equal to the number of particles in a correlation volume, and typically for room-temperature thermotropics has a value of order 100.

B. Lyotropics

We are using the term *lyotropic* to describe liquid crystals composed of immutable rodlike molecules dissolved in a solvent, i.e., colloidal suspensions, as opposed to the common usage of lyotropic to denote liquid crystals of self-assembling molecules such as micellar solutions. The first molecular theory of the isotropic-nematic (*I-N*) phase transition for lyotropics was developed during the 1940s by Onsager [10]. One of the systems studied by Onsager was a gas of long, thin rods. The pair-potential considered was that of hard-core repulsion which prevents two rods from occupying the same space simultaneously. Deviation from ideal-gas behavior was restricted to two-body interactions only, which is exact for low rod concentrations. Onsager's result was the prediction of a *I-N* transition in the absence of any attractive interactions between particles. In this system, where the pair potential is purely repulsive, the free energy of the system consists only of entropic terms. The phase transition is driven by a competition between the rotational entropy of the rods, which favors an isotropic phase and the entropy of packing, which favors aligned rods. At high rod concentrations the isotropic phase is unstable because the rods become highly interdigitated which dramatically decreases the translational entropy of the rods. At a critical concentration, which depends only on the axial ratio of the rods, the total entropy of the rods is maximized by becoming orientationally ordered. Onsager also treated the case of charged rods in an aqueous solvent by calculating an effective hard rod diameter due to the electrostatic repulsion between rods. His model qualitatively explains the observed behavior of charged rod suspensions, but quantitatively the theory, as discussed by Onsager, is only correct if the axial ratio is greater than about 100. For shorter rods the interactions greater than two-body ones become increasingly important.

The magnetic birefringence of the isotropic phase of a lyotropic liquid crystal was first discussed by Straley [28] in a thorough review article of the experiments and theory of lyotropics as of 1973. Straley showed that the magnetic birefringence of hard rods in the limit of zero field for the Onsager approximation is

$$\frac{\Delta n}{cH^2} = \frac{\Delta N'_{\rm sat}\Delta\chi}{15kT(1-c/c^*)} \quad (3a)$$

with $c^*=4/b$, where $b=\pi L^2 D/4$, the average excluded volume of a pair of rods in the isotropic phase, and L is the length and D the diameter of the rod. The maximum birefringence of the suspension is

$$\Delta n_{\rm sat} = c\Delta N'_{\rm sat} . \quad (3b)$$

Analogous to the thermotropic case, the birefringence diverges when the concentration c increases to the value of c^*. Before this occurs, the suspension becomes nematic, which in the Onsager model occurs at $c=3.3/b$. In this model, the specific field induced birefringence of Eqs. (3) is 5.7-fold greater at the *I-N* transition than when the concentration is zero.

The first study of pretransitional effects in lyotropics of rodlike molecules using magnetic-field-induced birefringence was performed by Nakamura and Okano [29]. The system investigated was the bacteriophage *fd*, a long, thin, and slightly flexible molecule. They studied both the magnetic susceptibility and the rotational diffusion of the rods in the isotropic phase over a wide concentration range for one ionic strength and constant temperature. The specific magnetic-field birefringence was observed to increase threefold from the dilute limit to near the *I-N* transition.

The temperature dependence of the induced birefringence reported by Photinos *et al.* and summarized in Eq. (1) is very intriguing. In our Introduction, we suggested that electrostatic repulsion is by far the most significant interparticle force in determinng phase behavior. Evidence supporting this claim is supplied by scattering experiments probing interparticle spatial correlations in the isotropic phase of TMV [5]. These experiments reveal spatial correlations consistent with a fluid of rods which maximizes the distance between rod surfaces. This causes the particles to be separated by such dis-

tances that van der Waals forces are very small [3] with respect to the electrostatic repulsion. In a suspension of hard rigid rods, the value T^* is zero. With rods interacting solely through electrostatic repulsion, the ground-state configuration at zero temperature would be a β-tungsten structure consisting of antiparallel alignment of the rods [5,30] and consequently T^* would be *negative.* One motivation for our study was to determine if the observed positive value of T^* arose from thermotropic pretransitional effects, or was a consequence of the temperature dependence of the single-particle properties parametrized in the product $\Delta N'_{\rm sat}\Delta\chi$.

C. Onsager theory for short, rigid, charged rods

As mentioned earlier, the Onsager approximation of including only two-body interactions is valid if the axial ratio exceeds about 100, and TMV has an axial ratio of about 15, far less than can be expected to be described accurately by Eq. (3). Rods of such small anisotropy require higher terms in the virial expansion of the free energy for hard rods developed by Onsager. The problem in extending the Onsager theory to take into account higher terms in the virial expansion is that there are no analytical expressions for the terms higher than the two-body term discussed by Onsager [10] and Straley [28], although there have been efforts to find an analytical expression for the excluded volume of three rods [31]. Thus, while the contribution of the higher-order virial terms to the magnetic birefringence has been derived by Photinos and Saupe [32], it is only possible to analytically evaluate the coefficient of the lowest-order concentration term.

There are several theoretical approaches to account for the higher virial terms in hard rod systems of small axial ratio. Instead of using an ideal gas as the reference state, the other choice is to use the liquid of hard spheres as the reference state and include the nematic interaction at the level of the second virial coefficient. Since there are many theories for the free energy of a hard sphere liquid, there is ample opportunity to form theories of short rod nematic phases. In particular, we mention the recent contribution by Sato and Teramoto [33], describing the isotropic-nematic transition in a suspension of charged spherocylinders. We also refer the reader to the recent review article of the Onsager model and its extensions by Vroege and Lekkerkerker [23]. However, here we extend the theory presented by Lee [34], which describes the free energy of a suspension of uncharged spherocylinders of arbitrary axial ratio, to include the effects of an external magnetic field and of charge on the spherocylinder.

A spherocylinder is composed of a cylinder of length L and diameter D, with each end of the cylinder capped by a hemisphere of diameter D. The theory of Lee essentially amounts to an interpolation between the accurate limiting theories of the Carnahan-Starling equation of state for hard spheres and the Onsager equation of state for infinitely long hard spherocylinders. The free energy of a liquid of hard spherocylinders proposed by Lee is

$$\frac{F}{NkT}=\frac{\mu_0(T)}{kT}+\ln c-1+\sigma(f)+\frac{\phi(4-3\phi)}{8(1-\phi)^2}\langle\bar{v}_{\rm excl}(\mathbf{a},\mathbf{a}')\rangle+E(f)\ , \tag{4}$$

where μ_0 is the chemical potential, c the concentration. The first three terms on the left side of Eq. (4) account for the free energy of an ideal gas. The next term, $\sigma(f)=\int f(\mathbf{a})\ln[4\pi f(\mathbf{a})]da$, arises from orientational entropy of the spherocylinders, where $f(\mathbf{a})$ is the normalized angular distribution function which represents the probability of a rod axis pointing in the direction $\mathbf{a}$. The fifth term arises from the entropy associated with the number of ways of packing rods of volume fraction ϕ, defined by $\phi=cV$, with V the volume of the spherocylinder, and $\bar{v}_{\rm excl}(\mathbf{a},\mathbf{a}')=v_{\rm excl}(\mathbf{a},\mathbf{a}')/V$, where $v_{\rm excl}(\mathbf{a},\mathbf{a}')$ is the volume excluded to two crossed spherocylinders with axes pointing in directions $\mathbf{a}$ and $\mathbf{a}'$. The angular brackets denote the orientational average. For long, thin ($L/D\gg1$), rigid, and hard (uncharged) rods the excluded volume $\bar{v}_{\rm excl}(\mathbf{a},\mathbf{a}')=8L|\sin\gamma|/\pi D$, where $\gamma(\mathbf{a},\mathbf{a}')$ is the angle between the cylinder axes.

When the cylinders are charged, the excluded volume is modified due to electrostatic repulsion. Onsager [10] argued that the principal effect of charge would be to increase the diameter of a long, thin rod from its physical diameter D, to an effective diameter $D_{\rm eff}=D(1+\delta)$, "by a modest multiple of the (Debye) screening distance $1/\kappa$." $D_{\rm eff}$ is calculated by finding the separation of the rods at which the energy of repulsion is of order kT when averaged over the isotropic angular distribution function in the isotropic phase. Following Onsager [10] and Stroobants, Lekkerkerker, and Odijk [35], the excluded volume for charged spherocylinders can be expressed as $\langle\bar{v}_{\rm excl}(\mathbf{a},\mathbf{a}')\rangle=8+3\pi\beta[\rho(f)+h\eta(f)]$ with $\beta=(L/D_{\rm eff})^2[\pi(1+3L/2D_{\rm eff})]^{-1}$ where the function $\rho(f)=(4/\pi)\langle|\sin\gamma(\mathbf{a},\mathbf{a}')|\rangle$, with the function

$$\eta(f)=\frac{4}{\pi}\langle-\sin\gamma(\mathbf{a},\mathbf{a}')\ln[\sin\gamma(\mathbf{a},\mathbf{a}')]\rangle-[\ln2-1/2]\rho(f)\ ,$$

and the parameter $h=1/\kappa D_{\rm eff}$. We assume that due to the effect of charge, both the cylindrical and spherical cap of the spherocylinder are increased by the same amount. We refer to Ref. [33] for a more in-depth treatment of this issue. The function $\eta(f)$ and constant h describe the destabilizing effect of the angular dependent electrostatic term in the free energy on the nematic phase which occurs because the potential energy is minimized when the rods axes are perpendicular. Stroobants, Lekkerkerker, and Odijk [35] and Odijk [36] have given a thorough discussion of the role of this effect on the isotropic-nematic transition, and have named the constant h the "twist" parameter.

The appropriate theory to calculate $D_{\rm eff}$ depends on the charge density of the polyelectrolyte. Weakly charged rods are described by Debye-Hückel theory, while highly charged rods require the Poisson-Boltzmann equation. A detailed discussion of these two cases is also found in the paper of Stroobants, Lekkerkerker, and Odijk [35]. They note that for TMV, the analytical ap-

proximation for the Poisson-Boltzmann equation given by Philip and Wooding [37] is accurate enough for determining D_{eff}. By numerically solving this equation and following the procedure outlined by Stroobants, Lekkerkerker, and Odijk, we obtained the effective diameter D_{eff}, and twisting constant h, of TMV as a function of ionic strength of the solution for a range of charge densities from 0.5 to 2.0 $e/\text{Å}$. Although the charge density is varied by a factor of 4, due to the nonlinear nature of the Poisson-Boltzmann equation, the effective diameter only changes by 10%. The results of the calculation are shown in Fig. 1.

The last term in Eq. (4) represents the free-energy contribution from a magnetic field given by

$$E(f)=-MS \ , \tag{5}$$

where $M=\Delta\chi H^2/3kT$, S is the order parameter, $S=\int f(\Omega)P_2(\theta)d\Omega$, θ the angle between the field and the rod axis, $d\Omega=2\pi\sin\theta d\theta$, and $P_2(\theta)=\frac{1}{2}(3\cos^2\theta-1)$. Finally, the free energy for short, charged spherocylinders is given by

$$\frac{F}{NkT}=\frac{\mu_0(T)}{kT}+\ln c-1+\sigma(f) + \frac{\phi(4-3\phi)}{(1-\phi)^2}\left\{1+\frac{3\pi}{8}\beta[\rho(f)+h\eta(f)]\right\}-MS \ . \tag{6}$$

By taking the appropriate limits this free energy reduces to ones previously published. For example, to pass to the hard rod limit let the Debye screening length go to zero. This sets $\delta=h=0$, and the free energy reduces to the one of Lee. To pass to the long, charged rod limit, keep κ^{-1} nonzero, let $D/L=0$ and take only the leading term in volume fraction ϕ. This gives the free energy discussed by Onsager [10] and Stroobants, Lekkerkerker, and Odijk [35].

The angular distribution function $f(\theta)$ can be expanded into Legendre polynomials and when the degree of alignment of the rods is small, as in the case of a weak magnetic field applied to the isotropic phase, only the lowest-order Legendre polynomial in $f(\theta)$ need be retained [28]. The normalized angular distribution in this case is

$$f(\theta)=\frac{1}{4\pi}[1+5SP_2(\theta)] \ . \tag{7}$$

The order parameter is a measure of the macroscopic or long-range angular order of the suspension. For an isotropic suspension in the absence of an aligning field, S is zero and the angular distribution is a constant.

The magnetic birefringence of a suspension of rods with a free energy given by Eq. (6) is easily calculated. In the circumstances where the angular distribution from Eq. (7) is valid, the free energy of Eq. (6) can be written as a function of S using $\sigma=5S^2/2$, $\rho=1-5S^2/8$, and $\eta=15S^2/32$. Then the order parameter which minimizes the free energy is found:

$$S=\frac{\Delta\chi H^2}{15kT}\frac{1}{1-\frac{c}{c^*}\frac{(1-\frac{3}{4}\phi)}{(1-\phi)^2}(1-\frac{3}{4}h)} \ . \tag{8}$$

The field-induced birefringence is simply the product of the order parameter and the birefringence of a perfectly aligned suspension of number concentration c:

$$\Delta n=\Delta n_{\text{sat}}S=c\Delta N'_{\text{sat}}S \ . \tag{9}$$

The order parameter becomes $S\propto[1-c(1-0.75h)/c^*]^{-1}$ in the limit of small c, and is exact for $L/D\gg1$, where c^* and Δn_{sat} are defined as in Eq. (3) but with D replaced by D_{eff}. The order parameter diverges at the concentration $c=c^*/(1-0.75h)$. This is the concentration for which a suspension of rods would become nematic by a second-order transition, if a first-order transition did not occur first, and is the bifurcation point of the Onsager theory as discussed by Kayser and Ravache [38], Odijk [36], and Stroobants, Lekkerkerker, and Odijk [35]. From this expression, we see that the electrostatic repulsion between TMV molecules affects the I-N transition in two opposing ways. First, by lowering the ionic strength, the effective diameter of the particle is increased, thus reducing the TMV concentration at the I-N transition. Second, the angular-dependent electrostatic potential acts to counteralign the particles, as characterized by the parameter h. Lowering the ionic strength increases h, and thus increases the concentration needed to have a stable nematic phase. Indeed, if h increases to $\frac{4}{3}$ the nematic phase is completely destabilized. From Fig. 1 we see that h is at most of order 0.1. Thus the balance of these opposing effects, for TMV, rests with the first case, and we observe that the concentrations of the I-N coexistence regime decrease as ionic strength decreases, as shown in Fig. 2.

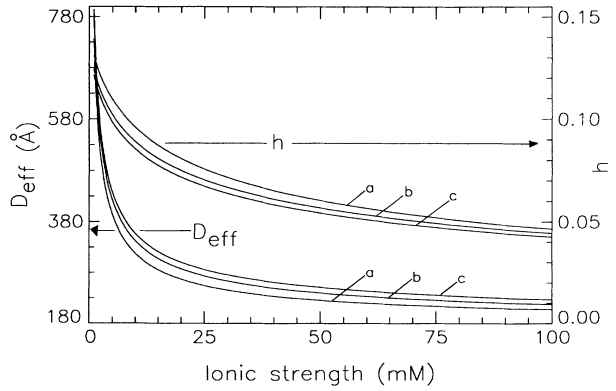

FIG. 1. Calculated effective diameter, D_{eff}, and twisting parameter, $h=1/\kappa D_{\text{eff}}$, for TMV as a function of ionic strength. D_{eff} (left ordinate) and h (right ordinate) are calculated from the Poisson-Boltzmann equation assuming a diameter of 180 Å and linear charge density of (a) 0.5 $e/\text{Å}$, (b) 1.0 $e/\text{Å}$, and (c) 2.0 $e/\text{Å}$.

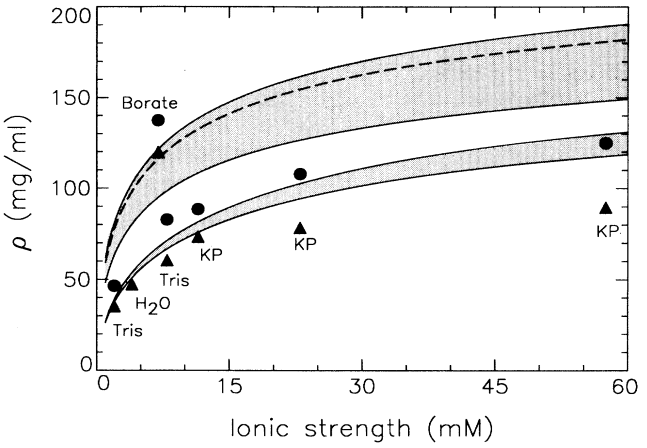

FIG. 2. The theoretical isotropic-nematic coexistence region for a spherocylinder of dimensions $L=2820$ Å and $D=180$ Å and linear charge density 2.0 e/Å are plotted for the Onsager theory given by Eqs. (14) (upper shaded region) and the theory of Lee as described in the text (lower shaded region). The dashed line is the calculated value of ρ^* and is identical for the two theories. The individual points correspond to measured values of ρ_i (▲) and ρ_n (●). All these samples were experimentally characterized to be monodisperse, including the TMV in borate buffer. Table II contains relevant information about these samples. The solvent of the TMV suspension is indicated next to the data points. Tris: TRIS-HCl, pH 8.0; KP: potassium phosphate, pH 7.2; Borate: borate buffer, pH 8.5; H_2O: unbuffered distilled water, pH 8.1.

D. Onsager theory for polydisperse suspensions

Next, we discuss the effect of polydispersity of the particles on the magnetic birefringence. Here we confine ourselves to consider the case of hard rods at low concentration, thus restricting ourselves to two-particle interactions, and furthermore neglect end effects in the excluded volume of two particles, as well as the "twisting" contribution of charge on the rods. We assume that the particles have aggregated end to end, which means a dimer is twice the length of a monomer but has the same diameter. In this case, both $\Delta N'_{\rm sat}$ [Eq. (3)] and $\Delta\chi$ will be proportional to the length of the particle. Observations of electron micrographs of aggregated TMV samples reveal only end-to-end aggregation. Even with these approximations, we should still be able to accurately describe the magnetic birefringence of TMV suspensions at low, but measurable, concentrations for samples that do not contain fragments of $L/D<10$. Similarly to the discussion of the magnetic birefringence of monodisperse spherocylinders, we write the free-energy difference between the solvent and the suspensions of spherocylinders in a magnetic field, postulate an angular distribution function, and solve for the order parameter that minimizes the free energy. Since we will minimize the free energy with respect to the order parameter, we only need to consider terms which contain the order parameter. Onsager [10] presented a qualitative discussion of this case, and later others [36,39] have examined aspects the effect of polydispersity on the I-N transition in the Onsager picture, although no complete theory has emerged. The angular-dependent terms of the free energy per particle are

$$\frac{\Delta F}{Nk_BT}=\sum_j \sigma_j x_j + bc\sum_j\sum_j x_j x_k q_j q_k \rho_{jk} - M\sum_j S_j x_j q_j \ . \tag{10}$$

The fraction of particles that have length q_jL is denoted by x_j, where q_j can take any positive value. If q_j is less than 1 the sample contains fragments, and if q_j is greater than 1 there are aggregates. The average excluded volume b is calculated for the reference particles of length L. The other parameters are the same as defined previously. As before, the free energy is expanded in terms of the order parameter where $\sigma_j=5S_j^2/2$ and $\rho_{jk}=1-5S_jS_k/8$. The free energy is minimized for each of the j species of rods. We are interested in calculating the induced birefringence which arises from the sum of the contributions to the total birefringence from each species of length Lq_j. The induced birefringence is

$$\Delta n=\sum_j \Delta n_j^{\rm sat} S_j \ , \tag{11}$$

where $\Delta n_j^{\rm sat}=\Delta n_1^{\rm sat} q_j x_j = c\Delta N_1'^{\rm sat} q_j x_j$ is the maximum possible, or saturation birefringence, from the rods of length Lq_j and number fraction x_j and $\Delta n_1^{\rm sat}$ is the birefringence of a monomer. Solving this set of coupled equations yields

$$\Delta n = c\frac{\Delta N_1'^{\rm sat}\Delta\chi_1 H^2}{15kT}\frac{\sum_j x_j q_j^2}{1-(c/c^*)\sum_j x_j q_j^2} \tag{12}$$

with c^* defined in Eq. (3). It is much easier to experimentally measure the mass density ρ, of particles rather than the number density ($c=N/V$), and these quantities are only proportional to each other for monodisperse samples. Absorption spectroscopy measures the mass density, while the number density must be inferred from difficult and inaccurate measurements of the particle size distribution. To convert Eq. (12) to units of mass per volume, we introduce the following quantities: m, the mass of a monomer of TMV of length 3000 Å, and M_j, the total mass of particles of length q_jL with $M_j=mNx_jq_j$. The mass density of the suspension is $\rho=\sum M_j/V$, the average mass density is $\bar\rho=\sum_i q_i M_i/V$, and $\overline{M}=\bar\rho/\rho$. The dimensionless ratio $\overline{M}$ is independent of concentration and is the ratio of the average mass of a particle to the monomer mass, m. With these definitions the induced specific birefringence becomes

$$\frac{\Delta n}{\rho}=\frac{\Delta N_1^{\rm sat}\Delta\chi_1 H^2}{15kT}\left[\frac{\overline{M}}{1-\frac{\rho}{\rho^*}\overline{M}}\right] \tag{13}$$

with $\rho^*=mc^*$ and $m\Delta N_1^{\rm sat}=\Delta N'^{\rm sat}$. Note that the parameters multiplying the term in parentheses are single-particle properties of the monomer, and are independent of polydispersity, ionic strength, and particle concentration.

IV. ISOTROPIC NEMATIC PHASE TRANSITION

Calculation of the coexistence concentrations requires equating the osmotic pressure and chemical potential of the two phases for the angular distribution, which minimizes the free energy of Eq. (4). To approximately describe the coexistence concentrations of monodisperse TMV, we use the results of Lee for hard spherocylinders. We model TMV as a spherocylinder of dimensions $L=2820$ Å and $D=180$ Å and of linear charge density in the range 0.5–2.0 electron/Å. The effective diameter D_{eff}, and twist parameter h, are calculated as a function of ionic strength as described above and plotted in Fig. 1, from which the aspect ratio of the particle $x=L/D_{\text{eff}}+1$, is obtained. Lee calculated the coexistence concentrations of the isotropic and nematic phases, c_i and c_n as a function of x, which we transform with the aid of Fig. 1 to be a function of ionic strength. We treat TMV as a hard particle with an aspect ratio that depends on ionic strength and neglect the contribution of "twist" to the *I-N* phase transition. Odijk [36] estimates, using a perturbation theory based on the Onsager limit, the magnitude of the twist effect in increasing the coexistence concentrations as $\partial c_i=2.37hc_i$ and $\partial c_n=3.01hc_n$. In this case, the coexistence concentrations are increased and the coexistence region is slightly widened. The values of c_i, c_n, and c^* as a function of ionic strength for the Onsager theory reported by Odijk [36] are described by the following equations:

$$c_i=\frac{3.29}{(1-0.675h)b}\ ,$$
$$c_n=\frac{4.19}{(1-0.73h)b}\ , \tag{14}$$
$$c^*=\frac{4}{(1-0.75h)b}\ .$$

The expressions for c^* are identical between the theory of Lee modified above and the Onsager theory, because the free energy in Eq. (4) reduces to the Onsager expression at low concentration.

The theory of Lee [34], which at some level contains higher virial coefficients, predicts transition concentrations lower than the Onsager theory. In other words, the higher coefficients act to stabilize the nematic phase. Excellent discussions of this are given by Straley [28] and Odijk [36]. The ratio of coexistence concentrations is smaller in the theory of Lee than for Eqs. (14). In Fig. 2 we plot the coexistence concentrations for TMV as calculated by Lee and Odijk as a function of ionic strength, using D_{eff} and h as shown in Fig. 1, and assuming a charge density of 2 e/Å.

How well does the theory of Lee describe concentrated suspensions of spherocylinders? Monte Carlo results for the osmotic pressure have been calculated for spherocylinders of several short lengths. We compare the virial coefficients between the theory of Lee and the Monte Carlo results of Monson and Rigby [40] in Table I. The values of B_2 for the theory of Lee are exact. Inspection of Table I reveals that the theory of Lee underestimates the third virial coefficient, and is close to the rest. However, within computational accuracy, the theory of Lee gives both the same osmotic pressure and transition concentration of the isotropic phase at the *I-N* transition as the Monte Carlo results of Frenkel [41] for the case of a spherocylinder of $L/D=5$. It seems in this case that the errors in the virial coefficients cancel. The theory of Lee has been extended to treat ellipsoids and compared well with Monte Carlo results [42] and has been applied to the nematic-smectic phase transition [43].

V. MATERIALS AND METHODS

Two strains of TMV were used in this study; one strain was the common strain (TMV) and the second was a mutant strain designated as U2 [44]. The structure and physical properties of the two viruses are similar. Both are composed of 2130 identical protein subunits arranged in a helix composed of 16 and $\frac{2}{3}$ units per turn of the helix, wound about a hollow, water-filled center of 40 Å diameter. The overall dimensions of the particles are 3000 Å in length, and (outer) diameter of 180 Å, with a total molecular weight of 4×10^7 g/M. The virus is negatively charged above the isoelectric point of *p*H 3.5, and there are 1–2 charges per protein unit at *p*H7. Besides protein, TMV contains a double strand of RNA running the entire length of the virus with three base pairs per protein subunit [45].

The TMV and one sample of the U2 strain were grown

TABLE I. Reduced virial coefficients for spherocylinders from the theory of Lee [34] (L), Monte Carlo results of Monson and Rigby [40] (MR), and Monte Carlo results of Frankel [41] (F). The second virial coefficient is exact.

L/D		0	1	2	3	4	5
B_2/V		4	4.60	5.50	6.46	7.43	8.41
B_3/B_2^2	L	0.6250	0.5435	0.4545	0.3868	0.3364	0.2973
	MR	0.6250	0.5832	0.5355	0.4896	0.4514	0.4196
	F						0.4346
B_4/B_2^3	L	0.2813	0.2127	0.1488	0.1078	0.0815	0.0636
	MR	0.2869	0.2312	0.1683	0.1183	0.0807	0.0531
	F						0.0669
B_5/B_2^4	L	0.1094	0.0860	0.0421	0.0259	0.0171	0.0118
	MR	0.1106	0.0822	0.0402	0.0228	0.0131	0.0126
	F						0.0115

and harvested by M. Cahoon at Brandeis University following the basic procedures of Boedeker and Simmons [46] and Kreibig and Wetter [8]. One sample (a generous amount) of the U2 strain was kindly supplied to us by G. Stubbs. The samples from Cahoon were stored in water and the Stubbs sample was stored in 10-mM sodium phosphate, pH 7.0. Shortly preceding the magnetic birefringence measurements, the samples were either used directly or placed in potassium phosphate buffer at pH 7.2. Two samples were dialyzed against this buffer and the third was prepared by diluting the TMV in a buffer and then reconcentrated by pelleting the virus in a centrifuge. Additional samples used in the measurement of the coexistence concentrations were dialyzed against TRIS-HCl at pH 8.0. These latter samples were used in a neutron scattering experiment measuring interparticle spatial correlations in concentrated isotropic TMV solutions as a function of ionic strength [5]. The conductivity of the samples were measured with a standard ac bridge meter (Seibold conductivity meter), and a calibration was made relating ionic strength of the buffer to the measured conductivity. The pH was measured with a standard meter equipped with a small probe. After dialysis, the sample concentration was adjusted such that approximately 90% of the solution was isotropic in coexistence with 10% nematic. Concentrations were determined spectrophotometrically using an extinction coefficient of 3.05 cm^2/mg at 265 nm wavelength [46].

With effort monodisperse preparations of TMV can be prepared according to the methods described above. Rapid aggregation occurs at high ionic strength (>100 mM) or at low pH ($<p$H 5), but will also occur over time at lower ionic strengths and higher values of pH. Stable monodisperse samples can be stored for a long time as concentrated suspensions in pure water. Fragmentation of TMV is induced by freezing or sonicating the suspensions. All our observations indicate that only end-to-end aggregation or fragmentation occurs, in other words the particles always have the same diameter. In this study, aggregation was induced by high ionic strength and fragmentation through freezing of the virus suspensions.

All magnetic birefringence measurements were performed at the Hochfeld Magnetlabor of the Max Planck Institut in Grenoble, France. The sample cells had either quartz or Teflon bodies with quartz windows. The cells had optical path lengths varying between 0.2 and 3.0 cm. These were placed in a temperature-stabilized sample holder in a Bitter magnet which had a small radial optical bore. The field-induced birefringence was measured using a combined photoelastic modulation and compensation technique [47]. Polarizer and analyzer were crossed and at 45° with respect to the field direction. The light source was a He-Ne laser ($\lambda=6328$ Å). The magnetic field was calculated by measuring the current passing through the magnet and separately determining the field-current relationship. The birefringence and magnetic field were registered on a personal computer from which the Cotton-Mouton (K_{CM}) constant was calculated where

$$K_{CM}=\frac{\Delta n}{\lambda H^2} \tag{15}$$

with λ the wavelength of light. The maximum attainable field in this magnet was 13.5 T [1 T$\equiv$1 Tesla $\equiv 10^4$ G (Gauss)] and the smallest measurable K_{CM} value was about $2\times10^{-8}\,T^{-2}\,cm^{-1}$.

VI. EXPERIMENTAL RESULTS

A. Magnetic birefringence: Low temperatures

In the preceding discussion, we have assumed that the degree of alignment by the magnetic field is small, which means that the field-induced birefringence should be proportional to H^2. In Fig. 3, the induced birefringence versus the square of the field is plotted for two concentrations of virus, and two temperatures. The proportionality between the square of the field and the birefringence is clearly shown. One can further note that the slope of these curves ($\Delta n/H^2$) decreases as concentration decreases or temperature increases.

The temperature dependence of the inverse specific magnetic susceptibility (ρ/K_{CM}) is shown in Fig. 4 for a range of concentrations of TMV in water with no added salt. Converting Eqs. (8) and (9) from number density (c) to mass density (ρ) yields

$$\frac{\rho}{K_{CM}}=\frac{\rho}{K_{CM}}\bigg|_{\rho=0}\left[1-\frac{\rho}{\rho^*}\frac{(1-\frac{3}{4}\phi)(1-\frac{3}{4}h)}{(1-\phi)^2}\right] \tag{16}$$

with

$$\frac{\rho}{K_{CM}}\bigg|_{\rho=0}=\frac{15kT\lambda}{\Delta N_{sat}\Delta\chi} \tag{17}$$

and the maximum possible birefringence $\Delta n_{sat}\equiv c\Delta N'_{sat}=\rho\Delta N_{sat}$. The conversion from number to mass density for monodisperse TMV is ρ[mg/m] $=c$[No./ml]4×10^{10} [mg/mol]$/6\times10^{23}$ [No./mol] and the mass, m, of a monomer of TMV is $m=\rho/c$. For the case of noninteracting particles the theory predicts that ρ/K_{CM} is a constant equal to $\rho/K_{CM}|_{\rho=0}$ for all concen-

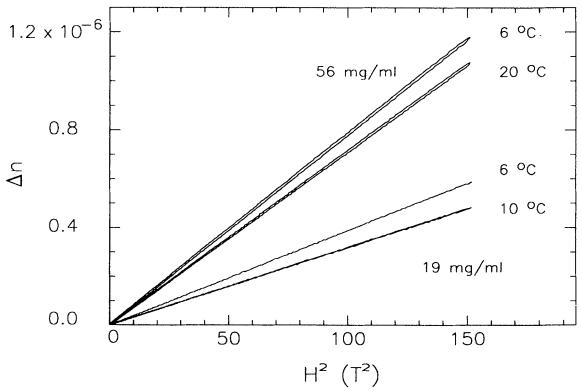

FIG. 3. Magnetic-field-induced birefringence (Δn) of TMV is proportional to the square of the field (H^2). The samples are in a 25-mM phosphate buffer at pH 7.2 and concentrations of 56 and 19 mg/ml and at the temperatures indicated. The traces are digitized recordings of sweeping the field up to and down from 12.3 T in 1 min.

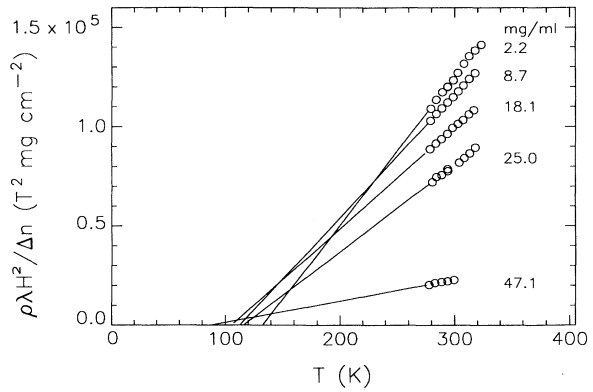

FIG. 4. The inverse specific magnetic susceptibility (ρ/K_{CM}) is shown as a function of temperature (T) for isotropic suspensions of TMV in unbuffered water. The highest concentration, 47 mg/ml, is in coexistence with the nematic phase. The values of ρ/K_{CM} were reversible within the temperature ranges shown for each concentration and fall on a line which extrapolates to zero at $T^*=115\pm20$ K.

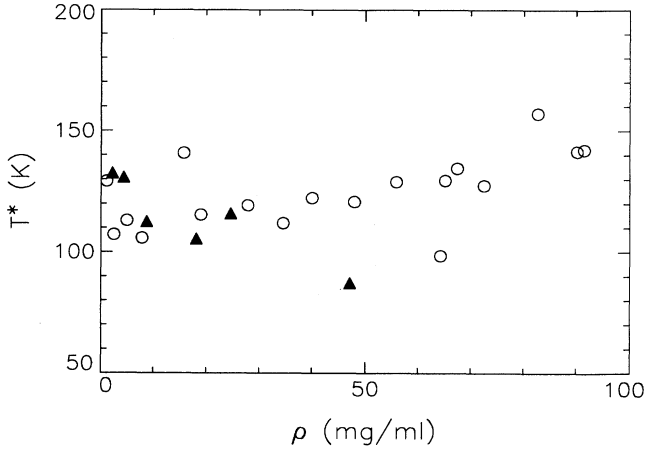

FIG. 5. The extrapolated temperature (T^*) as obtained in Fig. 4 is shown as a function of concentration for TMV in 25 mM phosphate (○) and in unbuffered water (▲). The samples of highest concentration for each data set are in coexistence with the nematic phase. $T^*=120\pm20$ K independent of concentration and ionic strength.

trations. The data in Fig. 4 demonstrate that there is a concentration dependence to ρ/K_{CM}. For each concentration ρ, Eqs. (16) and (17) predict that the temperature dependence is proportional to T. In Fig. 4 we observe that

$$\left.\frac{\rho}{K_{MC}}\right|_{\rho=0} = A(T-T^*) \tag{18}$$

with $T^*=115\pm20$ K with A a constant. This is contrary to Eq. (17) which predicts that $T^*=0$ K. Is it reasonable to identify the temperature at which ρ/K_{CM} becomes zero with T^* of Eq. (2)? In a thermotropic, T^* corresponds to the temperature that the isotropic phase would turn liquid crystalline by a second-order phase transition, except that actually a first-order phase transition always occurs earlier. In this sample, and for the range of temperatures studied, the values of ρ/K_{CM} were reversible with cycling of temperature. In Fig. 5, T^* as a function of concentration for two different ionic strengths is shown. Over the entire concentration range at which TMV is in the isotropic phase, T^* stayed constant within the range of $T^*=120\pm20$ K. The concentration range was 1–90 mg/ml for TMV in 25 mM phosphate buffer at pH 7.2 and 2–45 mg/ml for TMV with no added salt at pH 7.2.

The observations that T^* is a constant independent of both concentration and ionic strength belie against the interpretation that the TMV suspension is behaving as a thermotropic. This is because a mean-field theory of thermotropics, such as the Maier-Saupe theory, relate T^* to an effective single-particle attractive potential [2,26]. Models of the pair potential for TMV have been discussed in the literature [48] and compared with experiment [49]. van der Waals attraction favors parallel alignment and a close approach of two rods, while in contrast, electrostatic repulsion favors perpendicular alignment and a large separation between rods. It would be a very unlikely coincidence if such a potential, which has a strong dependence on both concentration and ionic strength, predicted that T^* would be independent of these two variables. Indeed, one expects that T^* should go to zero in the limit of very dilute suspensions because potential of mean force vanishes.

B. *I-N* coexistence: Low temperature

The essential quality of a thermotropic liquid crystal is the ability of temperature to induce an *I-N* phase transition. Therefore, we studied the change in the ratio of the volume of the isotropic and nematic phases in a biphasic sample of TMV in a 25 mM potassium phosphate buffer as a function of temperature. The sample was sealed in a 1-mm-diam x-ray capillary and placed in a water bath, which was mounted on a microscope. The microscope was turned on its side so that the long axis of the capillary was vertical. The level of the meniscus between the isotropic and nematic phase was monitored as a function of temperature, and the sample was kept at a given temperature for 24 h. At the beginning of the experiment the nematic phase occupied 40% of the total volume of the sample. The virus concentration of the isotropic and nematic phases, respectively, were 89.5 and 124.9 mg/ml. In the range of temperature from 2 to 25 °C there was no observable change in the meniscus. A change of 1% would have been clearly seen with the magnification of the microscope. At higher temperatures different behavior was observed, which we discuss below.

C. Origin of nonzero T^*

There remains the question of the origin of the observed T-T^* behavior of ρ/K_{CM} shown in Fig. 4, if it is not due to cooperative thermotropic-type effects. Equations (8) and (9) describe the magnetic birefringence in

the dilute particle limit for rigid particles. However, if at least one of the single-particle properties, $\Delta N'_{\rm sat}$ [Eq. (3)] or $\Delta\chi$ is temperature dependent, then the observations could be explained. To explore this matter further we must discuss the relationship between the structure of TMV and $\Delta N_{\rm sat}$ and $\Delta\chi$.

The birefringence of TMV is mainly due to the shape of the virus and not to intrinsic birefringence of the constituent elements of the virus. Shape, or form birefringence occurs in particles composed of optically isotropic material, but whose shape is nonspherical. Maxwell [50] first calculated that the form birefringence ($\Delta n_{\rm sat}$) of a dilute solution of isotropic rods of number density c, of index of refraction $n_1=1.57$, volume V, and in a solvent (water) of index $n_0=1.33$ is

$$\Delta n_{\rm sat}=\frac{cV(n_1^2-n_0^2)^2}{2n_0(n_1^2+n_0^2)} . \tag{19}$$

The product cV is equal to the volume fraction of rods, or expressed in terms of the weight concentration (ρ) in mg/ml, and density of the word, $d=1.37$ g/ml, we have $cV=\rho/d$. Thus

$$\frac{\Delta n_{\rm sat}}{\rho}=3.1\times10^{-5}\text{ml/mg} . \tag{20}$$

A measurement of the relative contributions of form and intrinsic birefringence was performed by Lauffer [51] who observed the flow birefringence of TMV as a function of average index of refraction of the solution. At an index of refraction of 1.57, he observed the complete disappearance of the induced birefringence in accordance with Eq. (19). Any residue birefringence would be due to intrinsic birefringence, and within the resolution of his experiment, there was none observed. The upper limit on the intrinsic birefringence of TMV established by Lauffer was 1–2% of the birefringence of TMV suspended in water. There probably is some intrinsic birefringence to TMV since dried films of TMV are birefringent [52] and presumably, dried films are dense enough so that no form birefringence remains.

Lauffer did not measure the specific birefringence of TMV in his initial study. However, $\Delta n_{\rm sat}/\rho$ has been measured in dilute suspensions of TMV using electric birefringence [53] and the value obtained was $\Delta N_{\rm sat}=\Delta n_{\rm sat}/\rho=2.1\times10^{-5}$ ml/mg. The specific birefringence has also been measured in nematic liquid-crystal suspensions of TMV [17]. In this case, the birefringence of the nematic (Δn) was measured and the value of the saturation birefringence was obtained using the relation $\Delta n=S\Delta n_{\rm sat}$, where the order parameter (S) was separately measured using x-ray scattering. These measurements yielded $\Delta n_{\rm sat}/\rho=1.9\times10^{-5}$ ml/mg. If we take the average of these two measured values, we find $\Delta n_{\rm sat}/\rho=2.0\times10^{-5}$ ml/mg. That the calculated value of the form birefringence is somewhat higher than the measured birefringence is not too surprising due to the assumptions involved in the calculation.

The fact that $\Delta n_{\rm sat}$ arises mainly from form birefringence implies that any temperature-induced change in $\Delta n_{\rm sat}$ must be accompanied by a change in the macroscopic shape or volume of the particle. For example, if TMV was increasingly flexible with increasing temperature, then $\Delta n_{\rm sat}$ would decrease with temperature. Yet both static and dynamic light scattering measurements of TMV fail to detect flexibility [54]. Likewise, electron micrographs of TMV show the particles most frequently as straight rods, with at most only slight curvature, which may be attributed to the forces exerted by drying. Longer and thinner viruses, such as *fd*, are flexible as determined by light scattering and electron microscopy [54,55]. Thus we feel that the observed T-T^* dependence of $\rho/K_{\rm CM}$ is most probably due to temperature variation of $\Delta\chi$.

The corresponding contribution of the shape anisotropy to the anisotropy of the diamagnetic susceptibility is negligible when compared with typical diamagnetic anisotropies of chemical bonds. The contribution to $\Delta\chi$ for a single TMV molecule, due to the shape anisotropy ($\Delta\chi_{\rm form}$), in cgs units is approximately [56]

$$\Delta\chi_{\rm form}=4\pi\chi_p(\chi_s-\chi_p)V , \tag{21}$$

where χ_p and χ_s are, respectively, the volumetric diamagnetic susceptibilities for the particle and the solvent, and V is the volume of TMV calculated using $L=3000$ Å and $D=180$ Å. We estimate χ_p for TMV using the known amino acid composition of TMV [45] and the diamagnetic susceptibilities of the amino acids [57], finding $\chi_p=-7.4\times10^{-7}$. The susceptibility of water is $\chi_s=-7.2\times10^{-7}$. Using these values we find that $\Delta\chi_{\rm form}=1.4\times10^{-29}$ erg/G^2. We will see below that $\Delta\chi_{\rm form}$ is negligible compared with the measured $\Delta\chi$ of TMV, which is greater than 10^4 times the value of $\Delta\chi_{\rm form}$. Thus we conclude that $\Delta\chi$ arises from intrinsic bond anisotropies.

The proteins comprising native TMV can be induced to self-assemble in the absence of RNA under certain conditions [58]. We measured the magnetic birefringence for these protein aggregates and found that the Cotton-Mouton constant was negative. The birefringence of the same aggregates was measured to be positive. This implies that the positive value of $\Delta\chi$ obtained for the native TMV (protein plus RNA) is primarily due to the RNA. As mentioned in Sec. V, there are three base pairs of RNA per identical protein subunit [45]. The portion of the RNA with the largest magnitude of $\Delta\chi$ is the aromatic base. If the plane of this aromatic ring is parallel to the TMV axis then $\Delta\chi>0$ and if the plane of the ring is perpendicular to the axis then $\Delta\chi<0$. X-ray structural studies reveal two of the base pairs have their planes approximately parallel to the axis, while the third face is oriented perpendicular to the axis. Roughly speaking, this leads to a net positive $\Delta\chi$ of magnitude equal to one base pair per protein subunit. We will see in Sec. VI F that this is indeed the case.

Small variations in the angle of these base pairs with temperature could account for the observed behavior of the Cotton-Mouton constant as a function of temperature. Indeed, similar behavior has been observed with other filamentous viruses [59]. It is possible that the

RNA loosens with increasing temperature, while the protein structure remains rigid. We will discuss our experiments on the protein aggregates in a separate publication.

D. *I-N* coexistence: High temperature

When the biphasic sample of TMV in 25 m*M* phosphate buffer was heated to 50 °C, small birefringent droplets rapidly appeared in the isotropic phase. After 5 min at this temperature, the sample had the appearance of a white fog when observed under crossed polarizers. At this time the sample was cooled back down to 20 °C. The newly formed nematic material did not transform back into the isotropic phase, and it appeared that no new nematic phase was being created. Within 15 min after the temperature had reached 20 °C the newly formed birefringent domains had coalesced into fewer, larger nematic drops, which gradually settled out of the isotropic phase and were deposited on top of the meniscus. After 5 h the macroscopic phase separation was completed, and the nematic phase had increased to occupy 50% of the total volume. This increase in the volume of the nematic phase was irreversible; further cooling did nothing to alter the new meniscus level.

We suggest that the virus in this sample began to aggregate end to end at 50 °C, which increased the excluded volume of the particles. This then decreases the concentration necessary to form a nematic phase and explains the increase in the volume of the nematic phase. End-to-end aggregation is a well-known problem in preparing samples of TMV [46]. Much effort over the years has been devoted to developing procedures to circumvent the occurrence of end-to-end aggregation of the virus, but apparently due to the structure of the virus and its mode of self-assembly, there exists a delicate balance between having viruses of its native length and fragments or aggregates.

Magnetic birefringence measurements as a function of temperature were consistent with the assumption of temperature-induced particle aggregation. In Fig. 6 ρ/K_{CM} vs temperature is shown for TMV of 6 mg/ml in 25 m*M* phosphate buffer, *p*H 7.2. For temperatures less than 42 °C, ρ/K_{CM} was proportional to $T\text{-}T^*$ and was reversible. Above this temperature, ρ/K_{CM} began to decrease steadily with time. Upon cooling down to temperatures below 42 °C, it was found that ρ/K_{CM} was again reversible but the values of ρ/K_{CM} had decreased from the first temperature scan taken below 42 °C. Aggregates of TMV have a larger value of $\Delta\chi$ than monomers, so the Cotton-Mouton constant increases with aggregation. In Sec. III D on polydispersity we showed that for dilute samples K_{CM}/ρ is proportional to the weight average of the particle distribution [Eq. (13)] which increases with degree of aggregation; thus the value of ρ/K_{CM} of an initially monodisperse suspension will decrease after aggregation occurs.

The form of the deviation of ρ/K_{CM} from being proportional to $T\text{-}T^*$ was dependent on the particle concentration and ionic strength. In Fig. 7, ρ/K_{CM} vs temperature is shown for TMV of 3.5 mg/ml concentration in 5 m*M* phosphate buffer. In this case, ρ/K_{CM} increases irreversibly above about 45 °C. This is the opposite to what occurs with aggregating samples, and would be consistent with denaturation of the virus, or breaking of the chemical bonds that are responsible for the diamagnetic anisotropy of the particle.

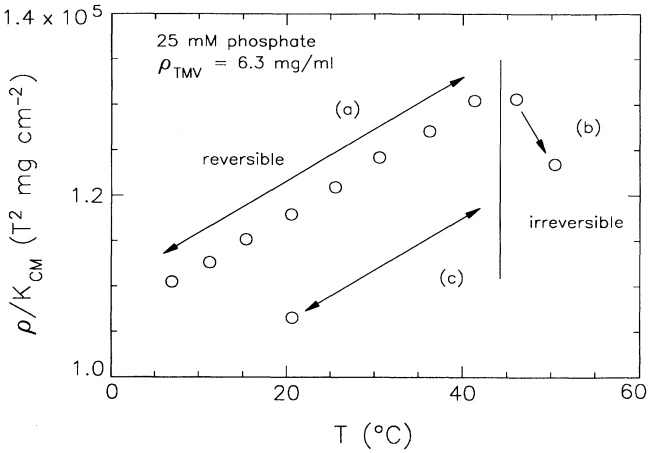

FIG. 6. The inverse specific magnetic susceptibility (ρ/K_{CM}) is shown as a function of temperature (T) for TMV of concentration 6.34 mg/ml in 25 m*M* phosphate buffer. In the limit of zero concentration ρ/K_{CM} is inversely proportional to the mass average of the suspension [Eq. (24)]. Curve (a) was reversible for temperatures lower than 42 °C. Above that temperature ρ/K_{CM} began to *decrease* irreversibly with time shown by curve (b). After 5 min, when the temperature was lowered below 40 °C, ρ/K_{CM} was again reversible with temperature as shown by curve (c) but ρ/K_{CM} had decreased below curve (a) implying that irreversible aggregation of the particles occurred.

At low ionic strengths the virus is charge stabilized

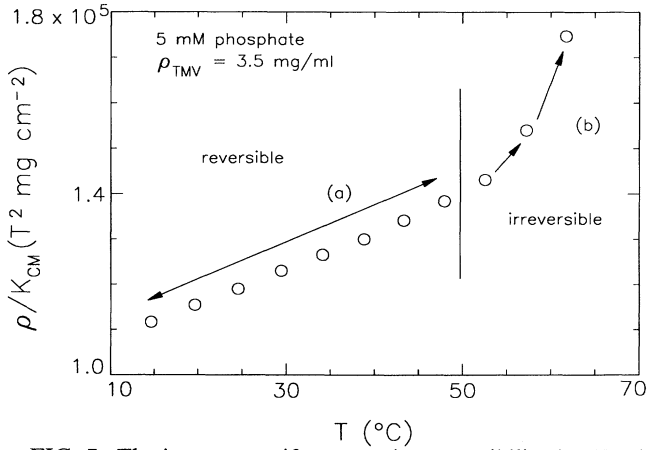

FIG. 7. The inverse specific magnetic susceptibility (ρ/K_{CM}) as a function of temperature (T) for TMV in 5 m*M* phosphate buffer at $\rho = 3.5$ mg/ml was reversible for temperatures lower than 45 °C [curve (a)]. Above that temperature ρ/K_{CM} began to *increase* irreversibly with time [curve (b)]. When the temperature was lowered below 40 °C ρ/CM was again reversible with temperature (not shown), but ρ/K_{CM} had increased above curve (a) implying that irreversible disintegration, or denaturation, of the particles occurred. This temperature dependence is opposite than that shown in Fig. 6.

against aggregation by a repulsive pair potential. Raising the temperature permits the TMV to mount this potential barrier and aggregation begins. The rate of irreversible aggregation in a given colloidal suspension is proportional to the concentration of the aggregating species. Thus at sufficiently low virus concentrations and low ionic strength, the denaturation process dominates at high temperatures while with higher concentrations and ionic strengths, aggregation proceeds faster than the denaturation.

To summarize the temperature dependence of TMV solutions, we observe that for the entire isotropic phase, ρ/K_{CM} is proportional to the T-T^* with T^* *independent of ionic strength and concentration,* as long as the temperature is low enough to prevent denaturation or aggregation of the virus. We find that $T^* = 120 \pm 20$ K for both species of virus. In addition, the coexistence of the isotropic and nematic phases is not effected by temperature. Therefore, we conclude that the nonzero value of T^* arises solely from internal changes in the structure of TMV, which is manifested in the temperature dependence of $\Delta\chi$.

E. Concentration and ionic strength: monodisperse suspensions

Having determined that T^* is a constant, it follows that to study the magnetic susceptibility as a function of concentration and ionic strength, it is only necessary to measure the Cotton-Mouton constant at one temperature for each concentration. In this study, all measurements were carried out at 20 °C. In Fig. 8, the measured ρ/K_{CM} values (individual points) as a function of concentration for four different ionic strengths are shown. The lowest ionic strength was achieved by placing ion-exchange resin in contact with the TMV solution, in which case the only ions present are the hydrogen counterions of TMV. The next highest ionic strength solution was from a TMV suspension prepared by the method of Boedtker and Simmons [46] and diluted with distilled water. The ionic strength which gave the best fit to theory [Eq. (16)] was estimated to be 4 mM, consistent with the measured conductivity (Table II). The last two samples were prepared by dialyzing against 5 and 25 mM potassium phosphate buffer at pH 7.2, and have an ionic strength of 11.5 and 57.5 mM, respectively. The concentrations of all samples, but the one in ion-exchange resin, span the entire isotropic range.

There are several features to note about the data. First, the value of ρ/K_{CM} at $\rho = 0$ is slightly different for the four samples, indicating a small, although nonnegligible, amount of polydispersity. Second, the concentration dependence of ρ/K_{CM} is a strong function of ionic strength. The excluded volume, $b = \pi L^2 D_{eff}/4$, which is proportional to the initial slope of the curves in Fig. 8, increases over 16 times from the case of the suspension in 25 mM phosphate buffer (57.5 mM), to the suspension kept in deionized water (resin) where the ionic strength is provided only by the counterions of TMV. Third, the three data sets which span the entire isotropic phase decrease faster than a linear function of concentration. If the rods had a large enough axial ratio (L/D) such that

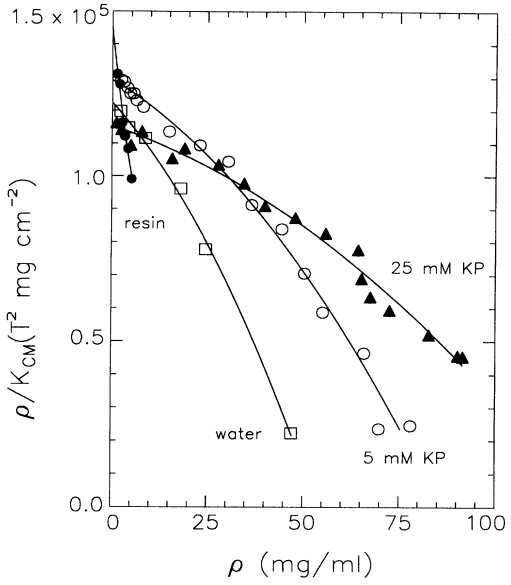

FIG. 8. The inverse specific magnetic susceptibility (ρ/K_{CM}) as a function of concentration (ρ) at constant temperature ($T = 20$ °C) was measured for four ionic strengths. All samples were monodisperse TMV. The symbols correspond to the following: ●, TMV in ion exchange resin; □, unbuffered water; ○, 5 mM potassium phosphate buffer, pH 7.2 (KP); and ▲, 25 mM KP. The solid lines are fits to Eq. (16) using parameters given in Table II. The last three samples cover the entire isotropic range. In the limit of zero concentration, $\rho/K_{CM} = 1.2 \pm 0.1 \times 10^5$ (T^2 mg cm^{-2}).

only two-body interactions were important, then ρ/K_{CM} would be described by Eq. (3) and would be linear in the TMV concentration. The observation of a nonlinear concentration dependence of ρ/K_{CM} implies that terms greater than the second virial coefficient are important in the I-N phase transition for TMV, which indeed was expected for rods with $L/D < 100$. Fourth, the highest concentration shown (except for the resin sample) is for the isotropic phase in coexistence with the nematic phase. The expected trend (Fig. 2), that the transition concentrations increase as ionic strength increases, is observed. Fifth, the ratio of the value of the maximum value of K_{CM}/ρ at the I-N transition to the minimum value of K_{CM}/ρ, which occurs in the limit of zero concentration, varies between 3 and 6 [see Fig. 9(a)]. This ratio is a measure of the number of particles in a correlation volume. We now proceed to discuss these points in more detail.

F. Cotton-Mouton constant of TMV and determination of $\Delta\chi$

The solid lines in Fig. 8 are fits to the inverse of the specific magnetic susceptibility (ρ/K_{CM}) derived in Eqs. (16) and (17). The low concentration limit of ρ/K_{CM} was obtained by extrapolating the data in Fig. 8 to $\rho = 0$. It is possible that $\rho/K_{CM}|_{\rho=0}$ could be a function of ionic strength and pH but we observe no systematic variation with these variables, and ascribe the experimental varia-

TABLE II. Monodisperse TMV was prepared in solutions of different ionic strengths. The explanation of the sample names follows. Borate: borate buffer of 50 mM boric acid at pH 8.5; KP: potassium phosphate buffer at pH 7.2; TRIS: TRIS-HCl buffer of pH 8.0; H_2O: an unbuffered sample; and resin: a suspension of TMV in contact with a mixed bed ion exchange resin. The measured quantities are (a) the value of ρ/K_{CM} in the limit of zero concentration; (b) $1+g_2$, the number of particles in an angular correlation volume [Eq. (23)] and plotted in Fig. 9(a), (c), (d), (e); ρ_i and ρ_n are the concentrations of the coexisting isotropic and nematic phases, respectively, (Fig. 2); (f) the analytical centrifuge data (Fig. 13) showed the particle length distribution to be discrete rather than continuous. The numbers separated by commas are the Svedburg constants, S_{Sved}, obtained from measurements at 3 mg/ml and then extrapolated to zero concentration using Eq. (27). Figure 12 shows the relation between S_{Sved} at zero concentration and particle length. (g) The parameter q is the ratio of the length of the particle obtained by the Svedburg measurement to the monomer length; (h) the symbol %, is the weight percent of material of length Lq; (i) $\bar{\rho}/\rho$ is the normalized mass average of the suspension obtained from the sedimentation measurements; (j) the pH; (k) the electrical conductivity, σ; (l) the ionic strength was calculated for the buffered samples knowing the pK and molarity of the buffer; (m) the Debye screening length, κ^{-1} (Å); (n) the effective TMV diameter, D_{eff}; (o) the twisting parameter, h; (p) the aspect ratio, $x=L/D_{eff}$. Entries (m), (n), (o), and (p) were calculated as described in the text using two values of the linear charge density of TMV. When two values are given, the first is for 0.5 e/Å and the second for 2.0 e/Å. The theoretical curves in Figs. 8 and 9 use these parameters. For the unbuffered H_2O and resin samples the effective diameters were found by fitting the data in Figs. 8 and 9 to Eq. (16) to obtain an effective diameter, and then calculating the ionic strength needed to give such a diameter for the two values of the charge density quoted above.

		Samples							
		50 mM Borate	25 mM KP	10 mM KP	5 mM KP	8 mM TRIS	H_2O	2 mM TRIS	Resin
Measured									
(a)	$\frac{\rho}{K_{CM}}$ (10^5 T^2 mg cm^{-2})		1.15±0.02		1.29±0.02	1.28±0.02	1.22±0.02	1.24±0.02	1.41±0.02
(b)	$1+g_2$		2.6		4.7		5.8		
(c)	ρ_i (mg/ml)	119.7	89.5	78.4	73.3	60.5	47.2	35.2	
(d)	ρ_n (mg/ml)	137.4	124.9	107.9	88.5	82.8		46.5	
(e)	ρ_n/ρ_i	1.15	1.40	1.38	1.21	1.37		1.32	
(f)	S_{Sved} (10^{-13} sec)		169, 204		157, 190		152		179
(g)	q		0.95, 1.59		0.79, 1.29		0.73		1.1
(h)	%		94, 6		90, 10		100		100
(i)	ρ/ρ		0.99		0.84		0.73		1.1
(j)	pH	8.5	7.2	7.2	7.2	8.0	8.1	8.0	
(k)	σ (10^{-3} Ω^{-1}cm^{-1})		3.8		1.0		0.29		
Calculated									
(l)	I (mM)	7	57.5	23	11.5	8	3.4–4.6	2	
(m)	κ^{-1} (Å)	36	12.7	20.1	28.4	34.1	52.3–45.0	68.2	
(n)	D_{eff} (Å)	353–395	221–245	259–291	306–344	339–380	450	552–603	2452
(o)	$h=1/\kappa D_{eff}$	0.10–0.092	0.057–0.052	0.078–0.069	0.093–0.083	0.10–0.090	0.12–0.10	0.12–0.11	
(p)	$X=L/D_{eff}$	8.0–7.1	12.8–11.5	10.9–9.7	9.2–8.2	8.3–7.4	6.3	5.1–4.7	1.2

tion in $\rho/K_{CM}|_{\rho=0}$ to arise from sample polydispersity. As seen from Table II and Fig. 8, the average value of $\rho/K_{CM}|_{\rho=0}$ at 20 °C is $1.2\pm0.1\times10^5$ $T^2\,mg\,cm^{-2}=2.9\times10^{30}\ g^2/cm^3$. In Sec. VI C we argued that the observed temperature dependence of ρ/K_{CM} described by Eq. (18) and shown in Figs. 4 and 5 arises from the temperature dependence of $\Delta\chi$. Thus Eqs. (17) and (18) together imply that

$$\Delta\chi=\Delta\chi_0\frac{T}{T-T^*} \tag{22}$$

with $\Delta\chi_0=15k\lambda/\Delta N_{sat}A$, a constant. Since $T^*=120$ K, this determines $A=705\ T^2\ mg\,cm^{-2}\ K^{-1}$ [Eq. (18)]. Then from Eq. (22) we find that $\Delta\chi_0=9.2\times10^{-25}\ J/T^2$. Thus, the susceptibility per particle at room temperature is $\Delta\chi(20\,°C)=1.6\times10^{-24}\ J/T^2=0.16\ Å^3$. Note that Eq. (22) is only valid for the temperature range of ~280–320 K. Dimensionless cgs electromagnetic units are commonly used in the field of liquid crystals and the conversion factor is given by $\Delta\chi[ergs/G^2]/V[cm^3]=\Delta\chi[1(cgs)]$, where V is the volume of the particle. A discussion of the units of $\Delta\chi$ is found in the review article of Maret and Dransfeld [60]. For pure TMV ($L=3000$ Å, $D=180$ Å) we find that the volumetric susceptibility is $\Delta\chi$ cgs $=2.0\times10^{-9}$ in dimensionless cgs units at 20 °C. For comparison, a typical low-molecular-weight liquid-crystal molecule, *MBBA* ($M_W=258$), has $\Delta\chi$ cgs $=1.2\times10^{-7}$ [61], a much greater value of the volumetric susceptibility than for TMV. *MBBA* is composed of two benzene rings, each of which has $\Delta\chi=-9.6\times10^{-28}\ J/T^2=-9.9\times10^{-7}$ cgs. TMV has a $\Delta\chi$ equivalent to 1566 aligned benzene rings or, because TMV is composed of 2130 identical proteins, 0.74 benzenes per protein subunit. This value is consistent with the expectation that $\Delta\chi$ arises primarily from the three RNA base pairs per protein subunit as argued in Sec. VI C. Since each subunit has a molecular weight of 18 000, the $\Delta\chi$ of TMV results from a nearly complete cancellation of the anisotropy of the diamagnetic susceptibilities of the chemical bonds which form the subunit. Photinos *et al.* [24] found a somewhat higher value for the Cotton-Mouton constant of TMV and $\Delta\chi=0.22\ Å^3$. Our experience is that there is a large degree of sample to sample variability of the Cotton-Mouton constant due to length polydispersity of TMV. We will discuss the issue of polydispersity in detail below.

G. Correlation volume

In linear-response theory, the susceptibility of a system to an external field is related to the correlations among the particles at zero field. For the case of magnetic-field alignment of a colloidal suspension in the isotropic phase, the amount of induced alignment is proportional to the degree of angular correlations between the rods at zero field [32]. A measure of the degree of angular correlation is [41]

$$1+g_2=\sum_{\substack{i,j\\ j\neq i}}P_2(\mathbf{a}_i\cdot\mathbf{a}_j)=\frac{S(\rho)}{S(0)}=\frac{K_{CM}/\rho}{K_{CM}/\rho|_{\rho=0}}\ , \tag{23}$$

where the sum ranges over all particles and S is the order parameter given by Eq. (8) and K_{CM}/ρ given by Eq. (16). The value of the sum ranges from 1 in the limit of $\rho=0$ and is equal to the total number of particles for a completely aligned nematic. There has been a detailed computer simulation on a fluid of spherocylinders with $L/D=5$ where $1+g_2$ has been calculated [41]. At the *I-N* transition the value of $1+g_2$ was difficult to determine due to the critical slowing down of the dynamics. One measurement on a system consisting of 576 particles after 20 000 trial moves per particle gave $1+g_2=5.8$ [41] while a longer run of 50 000 moves per particle yielded 2.6 [62]. In Fig. 9(a) the data of Frenkel [41,62] for $S(\rho)/S(0)$ or $1+g_2$ versus mass concentration (ρ) for spherocylinders with $L/D=5$ is plotted along with the values predicted by the theory of Lee for hard particles of the same aspect ratio. Note there are no free parameters when comparing the theory with the computer simulations. To compare with the TMV data, we see the length of these spherocylinders to have the TMV value of $L=2820$ Å.

The part of the specific magnetic birefringence that is due only to interparticular correlations $[S(\rho)/S(0)]$ can be obtained from the magnetic birefringence measurements by dividing K_{CM}/ρ, for finite concentration ρ, by the value of K_{CM}/ρ in the limit of $\rho=0$. In Fig. 9(a) $1+g_2$ is also plotted for the three samples which cover the entire isotropic phase in Fig. 8. The volume fraction was calculated using $\phi=cV_{eff}$ where V_{eff} was the volume of a spherocylinder of length $L=2820$ Å and diameter of D_{eff}. The number density was calculated from the measured weight concentrations. The solid lines in Figs. 9(a) and 9(b) were calculated using Eq. (16). The effective diameter, D_{eff}, and twisting parameter, h were calculated using the literature values of the physical dimensions of TMV, and the measured ionic strength of the solutions. The data of the 25 and 5 mM phosphate buffer suspensions were described well by the theory provided the charge density was between 0.5 and 2.0 e/Å, which fall in the range of the literature values for the charge density [11], so again, there are essentially no free parameters in the comparison of theory and experiment. The end points of the lines are the concentration at which the hard particle theory of Lee predicts a phase transition. These values are expected to be inaccurate since the effect of "twist" on the *I-N* transition is neglected. However, it should be emphasized that the twist term plays a much less important role than the effective diameter in determining the coexistence concentrations. Furthermore, the effect of twist *is* correctly incorporated into the theory of the induced birefringence in the isotropic phase.

The ionic strength of the sample diluted with pure water was unknown. In this case only, we fitted the ρ/K_{CM} data to Eq. (16) to obtain D_{eff}. The best fit yielded $D_{eff}=450$ Å. Assuming a linear charge density of 0.5 e/Å implied an ionic strength of 3.4 mM while a charge density of 2.0 e/Å implied an ionic strength of 4.6 mM (Fig. 1). These values were consistent with the measured electrical conductivity of the suspension (Table II). The average ionic strength value of 4 mM was used in Fig. 2

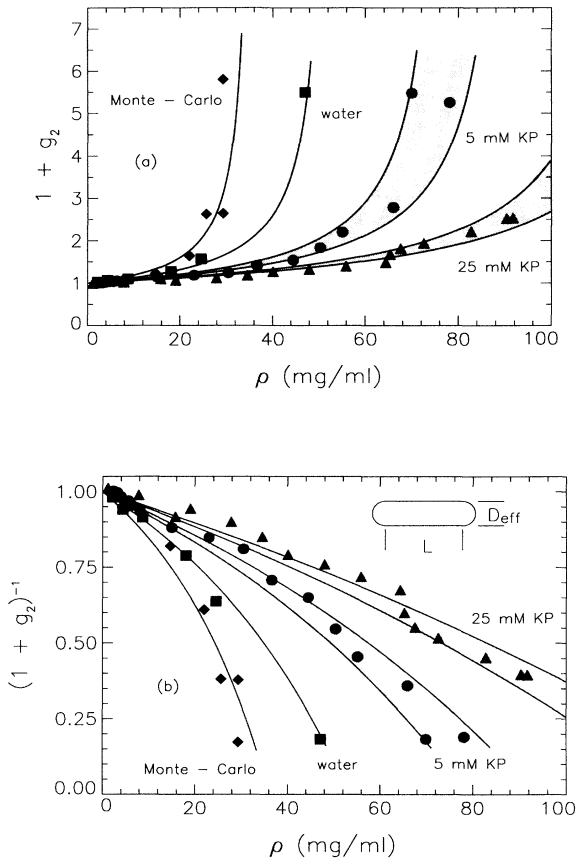

FIG. 9. (a) The normalized specific magnetic birefringence, $(K_{CM}/\rho)/(K_{CM}/\rho)|_{\rho=0}=1+g_2$ [Eqs. (16) and (23)] is shown as a function of weight concentration, ρ. This ratio is equal to the number of particles in a correlation volume. The solid lines are the theoretical predictions of Eqs. (16) and (23). The symbols represent the following: (♦), Monte Carlo data for hard spherocylinders of $L/D=5$, and the other samples are the same as in Fig. 8 and Table II; ■, unbuffered water; ●, 5 mM potassium phosphate buffer, pH 7.2 (KP); and ▲ , 25 mM KP. The theory for the Monte Carlo data [41] has no adjustable parameters. The theory curves for the two phosphate buffer samples were calculated assuming either 0.5 or 2.0 e/Å charge density for TMV and using the known ionic strength of the buffer. For a given TMV concentration, the correlations increase with increasing charge density. The ionic strength was not known for the unbuffered "water" sample. Here the ionic strength was a free parameter and the theory was fitted for the two values of the charge density given above. The ionic strength, effective diameter, and twisting constant for each sample is given in Table II. (b) The inverse of the normalized specific susceptibility $(\rho/K_{CM})/(\rho/K_{CM}|_{\rho=0})=(1+g_2)^{-1}$, which is the reciprocal of (a), is plotted as a function of TMV weight concentration, ρ. The main effect of varying ionic strength is to change the effective diameter, D_{eff}. The ratio of TMV length, L, to D_{eff} varies from 5 for the Monte Carlo data [41] to about 12 for the 25 mM KP sample (see Table II). Curvature in $(1+g_2)^{-1}$ vs ρ implies the contribution to the free energy of terms involving more than two-body interactions. This is predicted by the Onsager theory [Eq. (3)] to occur for rods of aspect ratio less than about 100.

in the phase coexistence plot.

We measured that the ratio of the induced specific birefringence at the I-N transition and the induced specific birefringence in the limit of zero concentration varies between 2.6 (57.5 mM) and 5.8 (3.3 mM), for the nearly monodisperse samples of Fig. 8 and Table II. The theory of Lee [34] for hard spherocylinders predicts $1+g_2$ varies between 7.8, for short particles of $L/D=1.75$ (the smallest aspect ratio at which a nematic phase occurs), and monotonously decreases to the Onsager limit of 5.7, when $L/D>100$. Including the effect of charge through the introduction of the twist parameter h in Eq. (8) reduces the birefringence at a given concentration, but we expect that "twist" also increases the concentration of the I-N transition [Eqs. (14)]. Our measured values of the correlation volume $1+g_2$, at the I-N transition decrease as ionic strength is increased, or equivalently as the aspect ratio increases, following the trend of the theory of Lee but the measured values are somewhat less than predicted by the hard rod theory.

In Fig. 9(b) the quantity $(1+g_2)^{-1}$, the reciprocal of Fig. 9(a) is plotted. The Onsager theory, including only the second virial coefficient, would predict that $(1+g_2)^{-1}$ decreases linearly in concentration. The data in Fig. 9(b) systematically decreases somewhat faster.

In summary, the theory for the concentration dependence of the angular correlation volume presented above, which accounts for higher-order virial terms and the effects of charge, describes well many aspects of the data. The theory fits well the computer simulations with no adjustable parameters. The theory also fits well the experimental curves for which the ionic strength was known, with the charge density in the range of 0.5–2.0 e/Å, which is consistent with the literature values.

H. Coexistence concentrations

The concentrations of the isotropic and nematic phases in coexistence were measured for six monodisperse samples and two polydisperse samples. The concentrations of the coexisting phases, ionic strength, and pH are listed in Tables II and III and the phase diagram of the monodisperse samples is shown in Fig. 2. The measured coex-

TABLE III. Data characterizing the inverse specific magnetic birefringence and coexistence concentrations of the polydisperse samples of the virus U2 in 5-mM phosphate buffer (see Fig. 10). The values of $\rho/K_{CM}|\rho=0$ and ρ^* were obtained by fitting the low concentration part of ρ/K_{CM} of Fig. 10 to Eq. (13). The remaining notation is as in Table II.

Sample	U2 mM % No. 1 (aggregated)	U2 5 mM No. 2 (fragmented)
$\left.\frac{\rho}{K_{CM}}\right\|_{\rho=0}$ (T^2 mg cm^{-2})	4.67×10^4	1.12×10^5
ρ^* (mg/ml)	70	202
$1+g_2$	3.2	4.0
ρ_i (mg/ml)	48.2	90.2
ρ_n (mg/ml)	67.5	109
ρ_n/ρ_i	1.40	1.21

istence concentrations are significantly lower than the Onsager theory truncated at the second virial coefficients. The theoretical curves are calculated assuming a charge density of 2.0 $e/$Å. Lower values of the charge density will shift the coexistence regions to higher densities because the effective diameter decreases (weakly) with decreasing charge density. The ratio of weight concentration of the nematic to the isotropic varies in a nonsystematic way between 1.15 and 1.40 for the monodisperse samples. The theory of Lee predicts that for large L/D the ratio is 1.24, the value of the Onsager theory, and that this ratio monotonously approaches zero as L/D decreases towards 1.75. In Fig. 2, we see that the measured coexistence region is wider than predicted by the effective hard rod theory of Lee. This could be due to the neglect of the "twist" term in calculating the coexistence concentrations or a result of a small amount of sample polydispersity.

The coexistence concentrations for samples in borate buffer are much higher than for all the other samples. We have no explanation for this behavior, however, light scattering, analytical sedimentation, and electron microscopy measurements rule out the possibility of aggregation.

Recently, Sato and Teramoto [33] proposed a theoretical model of the *I-N* transition based on a scaled-particle theory, applicable to charged particles, such as TMV. They compared our data of the coexistence concentrations with their theory, using the value of 0.5 $e/$Å for the linear charge density. This value was previously used in calculating the coexistence concentrations [6], because we believed that this charge density gave the best fit between the predictions of the theory of Lee for both the measured coexistence concentrations of Fig. 2 and the magnetic birefringence data of Figs. 8 and 9. However, there was a computational error [63] in the calculation of the coexistence concentrations (but not the susceptibility calculation). After correcting our error, we now find, that a range of linear charge densities from 0.5 to 2.0 $e/$Å fit the susceptibility data, but we conclude that a charge density of 2.0 $e/$Å fits the coexistence data better than the lower value of 0.5 $e/$Å. We guess that agreement between the theory of Sato and Teramoto and our coexistence data will also improve when the higher charge density is used. Additionally, the higher value of 2.0 $e/$Å is closer to estimates of the charge density based on conductometric titration [11].

I. Aggregation of TMV at low ionic strength

If the concentration of TMV in contact with mixed bed ion exchange resins samples is increased beyond about 6 mg/ml, the samples become simultaneously birefringent and beautifully iridescent when viewed with white light. The iridescence was strongest when the direction of illumination and observation were confined to the plane perpendicular to the director, implying a large degree of interparticle correlation in the plane perpendicular to the rods axes. This is the opposite to what has previously been observed with iridescent TMV suspensions [7,8], where the Bragg planes were oriented perpendicular to the director, as in the case of smectic liquid crystals for which the interparticle correlations are parallel to the rod axis. The iridescent samples flowed easily, but did not reorient when placed in a 7 T magnetic field for several days. These samples also become irreversibly aggregated at the onset of iridescence, while at concentrations just below the transition they were stably monodisperse.

What is the explanation of this behavior? TMV is known to aggregate end to end when the *p*H falls below 6 [64]. For samples in contact with ion exchange resin the only counterions for the TMV molecules are hydrogen ions so the *p*H falls as TMV concentration is increased (if the TMV charge density stays constant). Perhaps above concentrations of 6 mg/ml, the *p*H is low enough to aggregate the TMV. Once aggregated the excluded volume increases rapidly ($b \sim L^2 D$), and the sample undergoes a phase transition to a highly ordered nematic phase.

J. Magnetic birefringence of polydisperse suspensions

Changing the particle size distribution from monodisperse to polydisperse by end-to-end aggregation or fragmentation of the virus has a strong effect on the isotropic to nematic phase transition. Recall that Eq. (13) predicts that

$$\frac{\rho}{\Delta n} \propto \frac{1}{\bar{M}} - \frac{\rho}{\rho^*} . \tag{24}$$

The quantity $\bar{M}$ is equal to the average mass of the particles divided by the monomer mass, m. The critical concentration $\rho^* = b/4m$ is the excluded volume of the monomer [Eq. (3)] divided by its mass and by definition is independent of aggregation. Figure 10 shows the inverse

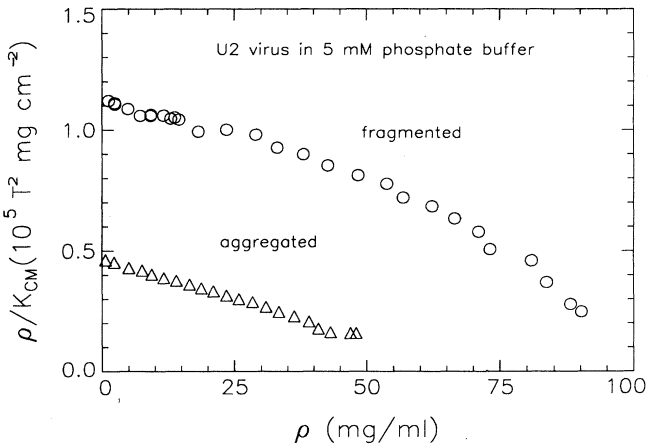

FIG. 10. The inverse specific susceptibility (ρ/K_{CM}) is shown as a function of weight concentration (ρ) for two samples of the mutant TMV species U2 of different degrees of polydispersity. The symbols are as follows: △, U2 in 5 m*M* potassium phosphate (KP) buffer, *p*H 7.2, aggregated; and ○, U2 in 5 m*M* KP buffer, fragmented. The initial slopes, coexistence concentrations, and characterization of the particle size distribution are contained in Tables III and IV. The theory [Eq. (24)] predicts the initial slopes of ρ/K_{CM} vs ρ should be independent of the particle size distribution. The highest concentration for each sample is in coexistence with the nematic phase.

of the specific magnetic susceptibility versus concentration for one partially fragmented and one partially aggregated sample of the U2 strain of TMV, and Table III contains the results of fitting the low concentration data to Eq. (13). Several features of Fig. 10 are notable. First, ρ/K_{CM} at $\rho=0$ varies with the degree of polydispersity of the sample. Second, the initial slopes of the curves for samples of different degree of polydispersity but the same ionic strength are equal, as predicted by theory [Eq. (24)]. Third, the ρ/K_{CM} data of the aggregated sample is linear in concentration, indicating that only the second virial coefficient is important. This is in contrast to the fragmented sample for which the ρ/K_{CM} data are nonlinear functions of ρ. Fourth, the transition concentrations for samples of identical ionic strength are larger for the fragmented samples than for the aggregated ones. Fifth, there is a plateau in ρ/K_{CM} for the aggregated sample near the *I-N* transition. This effect will be discussed in the next section.

K. Segregation and characterization of polydisperse samples

An important feature of polydisperse samples is the preferential segregation of longer particles into the nematic phase when in coexistence with an isotropic phase [7,39,65]. Characterization of the particle size distribution in each phase was performed for the fragmented sample of Fig. 10 using two techniques in addition to magnetic birefringence: electron microscopy and analytical sedimentation. Each of these techniques have their limitations, which we will attempt to indicate.

Electronmicrographs were made by Rob Ruigrok of the European Molecular Biology Laboratory, Grenoble, France of material taken from the coexisting isotropic and nematic phases of the fragmented U2 sample discussed in Sec. VI J above. Material was extracted from the isotropic and nematic phases with a pipet. Because the nematic phase is denser than the isotropic, the pipet first passed through the isotropic phase before reaching the nematic phase. Care was taken not to bring along any isotropic material into the nematic material and pipeting was done while observing the sample through crossed polarizers. The virus was placed on freshly cleaved mica at concentrations ranging between 0.03 and 0.3 mg/ml and then stained with uranyl acetate. The length distribution was measured from photographs and over 200 particles were measured for each distribution. Large velocity gradients and surface tension forces are present in the thin fluid film during the drying process, and this is thought to break the virus. Large aggregates are more probable to be present in clumps and are also more fragile, so we expect that length distributions measured with the electromicrograph (EM) will be biased towards smaller lengths. An example of EM photographs of material taken from the two coexisting phases, and the accompanying length histograms, are presented in Fig. 11 from the fragmented sample discussed in the previous section. These are the same samples for which the magnetic birefringence data was shown in Fig. 10. The mass averages obtained from the length histograms are given in Table IV. The width and appearance of virus in the two photographs is different because Fig. 11(a) is negatively stained while Fig. 11(c) is positively stained. However, this has little effect on the length measurement of

TABLE IV. Characterization of the particle-length distributions of a polydisperse U2 suspension in the coexisting isotropic and nematic phases using electron microscopy, analytical sedimentation, and magnetic birefringence. The sample used was the U2 virus identified as *fragmented* and discussed in Sec. VI K and Figs. 10, 11, and 13. The entries "ratio n/i" refer to the ratio of the mass average measured in the nematic phase (n) to the isotropic (i) phase using the following techniques: analytical sedimentation, electron microscopy, and magnetic birefringence. The specific magnetic birefringence K_{CM}/ρ, is measured in the limit of zero concentration and by Eq. (24) is proportional to the mass average of the suspension. The explanation for the symbols of the other rows is the same as for Table II. Fractionation of the heavier particles into the nematic phase is evident because the normalized mass average ($\bar{\rho}/\rho$) of the nematic is greater than the isotropic phase.

	U2 5 m*M* (fragmented)		
	Isotropic		Nematic
	Analytical sedimentation		
S_{Sved} (10^{-13} sec)	167, 177		177, 182, 196
q	0.9, 1.1		1.1, 1.2, 1.4
%	22, 78		20, 50, 30
ρ/ρ	1.0		1.2
ratio n/i		1.2	
	Electron microscopy		
ρ/ρ	0.8		1.6
ratio n/i		2.0	
	Magnetic birefringence		
$\frac{K_{CM}}{\rho}$ ($T^2\,mg^{-1}\,cm^2$)	9.1×10^{-6}		1.5×10^{-5}
ρ/ρ	1.1		1.8
ratio n/i		1.7	

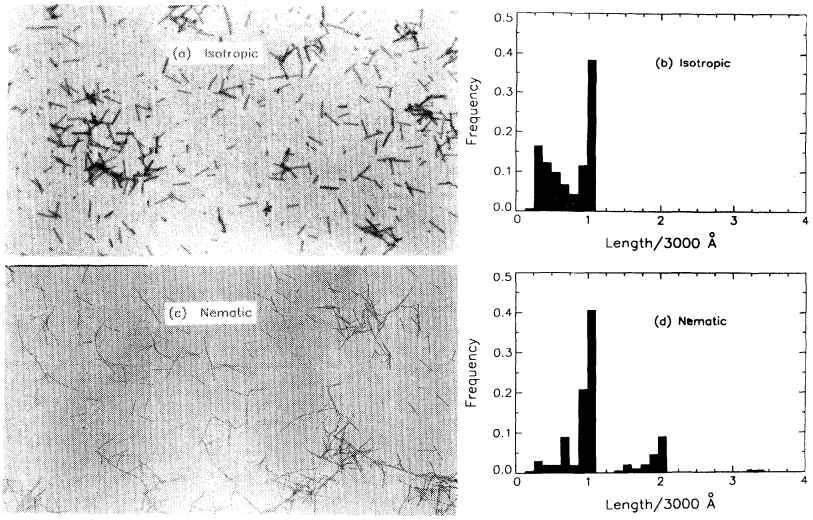

FIG. 11. Electronmicrographs of material taken from each of the coexisting isotropic and nematic phases showed segregation of the longer particles into the nematic phase. The photographs are from the U2 5 mM fragmented sample of Fig. 10. (a) Isotropic phase, (b) length histogram obtained from (a) in units of the monomer length (3000 Å), (c) nematic phase, and (d) length histogram of (c).

the virus. Not all the particles in these photographs were measured and a subjective decision to reject the ones in "clumps" was made.

The second technique used in characterizing the particle distribution was analytical sedimentation [46,66,67]. In this technique, a colloidal suspension is caused to sediment by application of a centrifugal force. The mass distribution of the suspension perpendicular to the rotation axis is measured as a function of time. Initially, before the centrifuge spins, the mass distribution is uniform. After centrifugation begins, the suspension sediments leaving behind a region devoid of particles. The rate of propagation of the depletion zone in the limit of zero-particle concentration is proportional to S_{Sved}, given by the Svedburg equation [67]

$$S_{\text{Sved}} = \frac{MD}{RT}(1 - V_{\text{sp}}\zeta) \tag{25}$$

with M the molecular weight, D the diffusion constant, R the universal gas constant, V_{sp} the specific volume (0.73 $\text{cm}^3\,\text{g}^{-1}$ for TMV), and ζ the density of the solvent. S_{Sved} is expressed in units of 10^{-13} s. The three quantities, S_{Sved}, M, and D, have been measured independently of each other at 20 °C with the respective values of 186×10^{-13} sec [46], 4×10^{7} g/mol [46], and 4.2×10^{-8} cm^2/s [68] and are consistent with the Svedburg equation.

To extract the mass distribution from analytical centrifugation measurements of the Svedburg constant of polydisperse samples, it is necessary to know how both the mass and the diffusion constant depend on aggregation. We only observe end-to-end aggregation of TMV in the EM photographs, so we assume the mass of the aggregated TMV particles is proportional to the length of the particle. If the length is q times the monomer length, then the mass will be Mq. The diffusion constant of long rods as a function of aspect ratio been derived theoretically by several authors. We use the formulas of Broersma [69] given by

$$D = \frac{kT}{6\pi\eta Lq}(2\sigma - \gamma_{\parallel} - \gamma_{\perp}) \tag{26}$$

with $\sigma = \ln(2qL/D)$, and $\gamma_{\parallel}$ and $\gamma_{\perp}$ are a series in powers of $1/\sigma$. Thus for the case of rods the Svedburg constant [Eq. (25)] S_{Sved}, is only logarithmically dependent on the ratio $q = L/D$. The calculated Svedburg constant as a function of q is shown in Fig. 12. Equation 26 predicts the Svedburg constant of TMV to be 176×10^{-13} s.

At finite concentrations, deviations from the Svedburg equation are observed, which arise from several factors. Perhaps most important is the hydrodynamic interaction between particles. The flow of solvent from the sedimenting particles retards the descent of particles upstream, resulting in lower values of S_{Sved} as the concentration is increased. A second independent contribution is the concentration dependence of the diffusion constant, which decreases as the concentration is increased. The concentration dependence of S_{Sved} for monodisperse TMV has been measured [46] and for concentrations below 5 mg/ml is

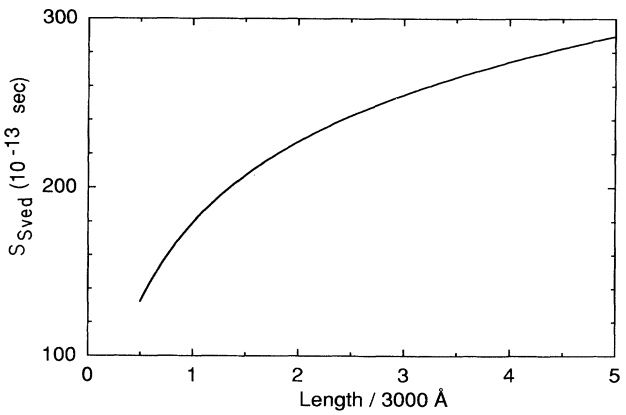

FIG. 12. The Svedburg constant for rods of the diameter of TMV, but of length 0.5–5.0 times that of TMV is calculated using Eqs. (25) and (26).

$$S_{\text{Sved}} = \frac{1000}{\rho 0.18 + 5.32} \tag{27}$$

with ρ the TMV concentration in mg/ml. However, the correction term describing finite concentration effects on S_{Sved} has not been measured for TMV particles of arbitrary length, nor is there any theory to describe the length dependence of this coefficient. This restricts meaningful measurements of the particle size distribution to low concentrations. Centrifugation measurements of all the samples were made at either concentrations of 0.3 or 3.0 mg/ml. The low concentration measurements were made using ultraviolet absorption. The logarithm of the ratio of transmitted to incident light intensity is the optical density and is proportional to the mass concentration. The higher concentration measurements used a Schlieren technique which gives a signal proportional to the rate of change of mass concentration with distance $(d\rho/dx)$.

Analytical centrifugation is not without its limitations. From Fig. 12 one sees that the Svedburg constant increases very slowly with q. This results in the inability to separate aggregates higher than dimers from the suspension in the time that it takes for the heavy particles to traverse the length of the cell. Another distortion of the size distributions that occurs in polydisperse samples arises from the concentration dependence of the sedimentation rate. If a centrifuging sample contains material with different sedimentation rates, then after spinning for some time there will be a region containing slow (small) particles but depleted of the fast (large) ones and a region containing both the slow and fast particles. The region containing only slow particles has a lower particle concentration than the region which has both species. The sedimentation rate of the slow particles will be greater in the low concentration zone due to the concentration dependence of S_{Sved} which causes a pile-up of the slow particles at the boundary between the two zones. This is known as the "Johnston-Ogston effect" [67] and results in the distortion of the mass distribution of polydisperse samples. If there are small amounts of fragments (aggregates) then these components are overweighted (underweighted) in the mass distribution.

Two uv analytical centrifuge scans of the fragmented sample whose length distribution was obtained with electron microscopy and shown in Fig. 11 is shown in Figs. 13(a) and 13(b). The material in Fig. 13(a) came from the isotropic phase in coexistence with the nematic phase, and in Fig. 13(b) the material came from the coexisting nematic phase. The family of traces are taken at successive times beginning from the left. The vertical bar at the right edge of each trace is the cell bottom. Each step in the absorbance traces indicates the boundary of one of the sedimenting species. The isotropic sample contains some fragments and monomers of TMV while the nematic sample shows three steps corresponding to fragments, monomers, and aggregates.

The magnetic birefringence measurement itself offers a method of characterizing polydispersity. The low concentration limit of K_{CM}/ρ is predicted to be proportional to the mass average of the distribution. Therefore the ratio of K_{CM}/ρ measured in the nematic and isotropic phases is equal to the ratio of the mass average of the particle size distribution in these two phases. For the fragmented sample discussed earlier, the mass average as measured by the magnetic birefringence is compared with the mass average obtained by centrifugation and electron microscopy in Table IV. The electron microscopy and Cotton-Mouton measurements are in closer agreement than the centrifugation measurements, perhaps due to the difficulty in interpreting centrifuge data from mixtures. All measurements were performed on coexisting samples that were approximately 90% isotropic and 10% nematic.

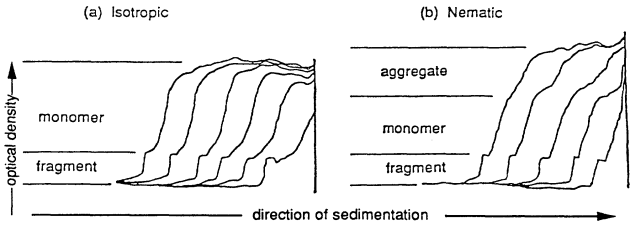

FIG. 13. Ultraviolet absorbence scans through sedimenting samples of material taken from coexisting isotropic and nematic phases of the U2 5 mM fragmented sample (same as in Figs. 10 and 11). The traces in (a) are from material taken from the isotropic phase and in (b) the material is from the nematic phase. The ordinate (optical density at 280 nm) is proportional to the total material in the cell and the abscissa is proportional to the distance perpendicular from the centrifuge rotation axis. Scans from left to right are at progressively later times, and show the material sedimenting towards the bottom of the cell. Each step in a scan is caused by a species of material that sediments at different rates. The position of each step is as a function of time is used to determine the Svedburg constant and is related to the length of the particles through Eqs. (25)–(27) and summarized in Fig. 12. The height of each step is proportional to the weight concentration of each species. The measured Svedburg constant and weight percentage of the species are presented in Table IV. In the isotropic phase (a) two steps are seen, corresponding to a lighter fragment and heavier monomer. In the nematic phase (b) three steps are observed, the fragments and monomer fractions as in the isotropic phase and additionally a heavier aggregate, which has preferentially segregated to the nematic phase.

In summary, a significant segregation of longer rods into the coexisting nematic phase of a polydisperse sample is observed. Note that segregation of the fragments did not occur. Independent measurements of the average mass of the particle size distribution using electronmicroscopy and analytical centrifugation support the interpretation that the specific magnetic birefringence measurements are proportional to the average mass of a polydisperse solution.

L. Magnetic birefringence of coexisting, polydisperse samples

In Fig. 10 the magnetic susceptibility of the aggregated sample as a function of concentration is well described by Eq. (24), implying that only two-particle interactions are significant. In contrast, the fragmented sample in Fig. 10

requires higher-order terms in concentration, as expected for shorter particles.

The ρ/K_{CM} data for the aggregated sample in 5 mM phosphate exhibits strange behavior in the vicinity of the I-N transition. Over a range of concentration of about 20% of ρ_i there is no change in ρ/K_{CM} with concentration. We offer the following possible explanation. As discussed in the previous section, polydisperse liquid crystals have different length distributions in the coexisting phases with the longer lengths preferentially segregating to the nematic phase. We measured the most concentrated samples with about 10% nematic in coexistence with 90% isotropic. In these circumstances there was significant segregation of the long particles into the nematic phase. The samples at lower concentrations were prepared by diluting the biphasic sample to what appeared to be a uniform isotropic phase. The single-phase isotropic material thus created has a different particle size distribution, with a greater mass average length, than the isotropic phase in coexistence with the nematic phase. Apparently, the decrease in concentration is compensated for by the increase in average excluded volume.

A typical example of the induced birefringence as a function of field for a sample of concentration near the I-N transition is shown in Fig. 14 for the 5 mM aggregated sample of Fig. 10. These measurements were taken by sweeping the field from 0 to 12.3 T in about 30 s and back to 0 T again at the same rate. The first time that the sample is exposed to the field is shown in Fig. 14(a). The slope $\Delta n/H^2$ for low values of H^2 is greater than the slope for high values of H^2 for the first time the field is increased from zero. On reducing the field this slope is a constant, as expected for an isotropic sample, but after the field had reached zero there was some residual birefringence, which slowly decreased with time. In Fig. 14(b) the field is swept from 0 to 12.3 T immediately after completion of the first sweep shown in Fig. 14(a). An offset of 5×10^{-6} in Δn was subtracted from the data for clarity of display. The induced birefringence in this case was as expected for an isotropic sample.

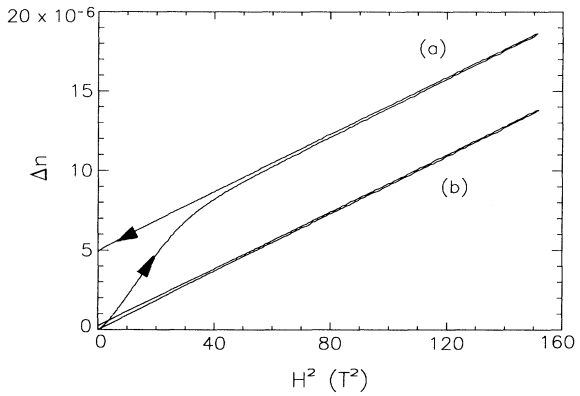

FIG. 14. The magnetic-field-induced birefringence as a function of field for isotropic samples near the nematic phase transition which contained small droplets of nematic. Curve (a) is the first field sweep of the sample. The nematic portion of the sample produces a large birefringence at low fields due to the aligning of the highly birefringent droplets and saturates at about 1 T. There is some residual birefringence after the field has been rapidly swept back to zero, because the alignment of the droplets persists for some minutes. The time to go up to and down from 12.3 T was about one minute. A subsequent field sweep rapidly following the first, shown in curve (b), behaves similarly to purely isotropic samples (Fig. 3) because the sweep time is faster than the orientational relaxation time of the nematic. For clarity of display, curve (b) was displaced to the origin. The amount of nematic material necessary to account for the residual birefringence seen at the end of the first scan [curve (a)] is less than 1% of the sample.

The observation of a birefringence signal at zero field implies that there is some nematic phase present. The time constant for the decay of this residual birefringence at zero field was consistent with the rotational diffusion of 100-μm-long rods. An examination of the suspension with optical microscopy showed there were a few birefringent anisotropic droplets of this size. A small amount of nematic droplets in suspension contribute a huge signal to the birefringence since the nematic phase has an order parameter of $S=0.9$ [17]. The magnitude of the residual birefringence in Fig. 14 is $\Delta n_{sat}=5\times10^{-6}$. The concentration of the nematic phase of this sample was 67.5 mg/ml. The birefringence of the nematic phase of this sample can be calculated using the value of $\Delta N_{sat}=2\times10^{-5}$ ml/mg. Given the order parameter and nematic concentration just mentioned yields $\Delta n=1.2\times10^{-3}$. If the residual birefringence of Fig. 14 is due to nematic droplets it follows that only 0.4% of the sample was nematic. Clearly magnetic birefringence is very sensitive to detection of the nematic phase.

The order parameter of the nematic phase is only weakly dependent on the applied field strength. We measured the increase in birefringence of a nematic sample of TMV in water at a concentration of 68 mg/ml as a function of field. The increase in birefringence measured from 4 to 12 T was linear in field as predicted for the quenching of thermal fluctuations of the nematic director [61] and increased by only one part in 10^{-4} per 1 T.

The principle effect of the magnetic field on the nematic droplets is to align them along the field, which occurs in the range 1–2 T. Above several tesla, the magnetic susceptibility of the isotropic portion can be measured from the response of the birefringence to higher fields, or from the slope of Δn vs H^2 for decreasing fields if the rate of change of field is much faster than the rotation of the nematic droplets, as in Fig. 14. We found that the susceptibility determined this way was independent of the amount of nematic droplets in suspension. Finally, we also observed that gentle centrifugation of the suspension removed most of the droplets.

Without centrifugation, the droplets were present even after waiting 24 h after diluting the macroscopically biphasic sample, and were observed until the concentration of the sample was about 20% less than the measured coexistence concentration of the isotropic, ρ_i. Thus the effect of polydispersity is to create a range of coexistence concentrations as the volume ratio of the two phases changes. There is an analogous effect in thermotropics. Monodisperse single component thermotropics cannot

have two phases in coexistence (Gibbs phase rule), while polydisperse thermotropics have coexisting phases for a range of temperatures which grows with increasing polydispersity.

VII. CONCLUSIONS

Isotropic suspensions of anisotropic molecules build up both spatial and angular local order with increasing concentration and eventually undergo an isotropic-nematic (*I-N*) phase transition. In this paper, we have measured the magnetic birefringence of aqueous suspensions of TMV as a function of temperature, concentration, ionic strength, and sample polydispersity over the entire isotropic range. The specific magnetic susceptibility, $\Delta n/\rho$, of the isotropic phase was calculated using an extension of the Onsager theory and related to the magnitude of angular correlations between particles. The measured values of the concentration-dependent part of the inverse specific Cotton-Mouton constant, ρ/K_{CM}, were in close agreement to theory with essentially no free parameters. The number of particles in a correlation volume at the *I-N* transition was in the range 3–6.

The extrapolation temperature T^* obtained from ρ/K_{CM} measurements of TMV suspensions was observed to be insensitive to both TMV concentration and ionic strength. Furthermore, the isotropic to nematic phase transition was measured to be independent of temperature. These observations are consistent with an interparticle potential and angular correlation length that are temperature independent, and a temperature dependent $\Delta\chi$ of TMV. The athermal nature of these phenomena are predicted by the Onsager model, which ignores attractive interparticle interactions.

The *I-N* coexistence region was measured as a function of ionic strength for monodisperse samples. The nematic boundary was close to the predictions of the hard spherocylinder theory of Lee, where the effective diameter of TMV was computed using the Poisson-Boltzmann equation. The measured isotropic branch was lower than predicted by theory, and the measured coexistence region was wider than predicted by the hard spherocylinder model.

Magnetic birefringence and coexistence concentration measurements were made for a fragmented and an aggregated sample of the same ionic strength. An expression for the leading terms of the concentration dependence of the magnetic birefringence of polydisperse samples was derived, and compared well with measurements. The phase behavior of the polydisperse samples was different than the monodisperse ones. Segregation of aggregated particles into the nematic phase of coexisting samples was observed, but segregation of fragments was not observed, and particle length distributions were determined using different techniques.

ACKNOWLEDGMENTS

S. F. would like to thank the NSF, Grants No. INT-8603303 and No. DMR-459850, and the Deutsche Forschungsgemeinschaft for financial support. We acknowledge illuminating discussions with R. B. Meyer, S. D. Lee, and T. J. Sluckin. We gratefully acknowledge the support of the European Molecular Biology Laboratories of Grenoble, France, for extensive use of their chemistry laboratories, electron microscopy facilities, and analytical centrifuge. Without their cooperation and technical assistance, this project could not have been completed.

*Permanent address: Martin Fisher School of Physics, Brandeis University, Waltham, MA 02254.

[1] J.-P. Hansen and I. R. McDonald, *Theory of Simple Liquids,* 2nd ed. (Academic, New York, 1986).
[2] W. M. Gelbart, J. Phys. Chem. **86**, 4298 (1982).
[3] V. A. Parsegian and S. L. Brenner, Nature (London) **259**, 632 (1976).
[4] D. Frenkel and B. M. Mulder, Mol. Phys. Lett. **52**, 1171 (1985); D. Frenkel, Mol. Phys. **60**, 1 (1987); M. P. Allen and D. Frenkel, Phys. Rev. Lett. **58**, 1748 (1987); and A. Stroobants, H. N. W. Lekkerkerker, and D. Frenkel, Phys. Rev. A **36**, 2929 (1987).
[5] E. E. Maier, R. Krause, M. Deggelmann, M. Hagebuchle, R. Weber, and S. Fraden, Macromolecules **25**, 1125 (1992).
[6] S. Fraden, G. Maret, D. L. D. Caspar, and R. B. Meyer, Phys. Rev. Lett. **63**, 2068 (1989).
[7] G. Oster, J. Gen. Physiol. **33**, 445 (1950).
[8] U. Kreibig and C. Wetter, Z. Naturforsch. Teil. **35**, 750 (1980).
[9] X. Wen, R. B. Meyer, and D. L. D. Caspar, Phys. Rev. Lett. **63**, 2760 (1989).
[10] L. Onsager, Ann. N.Y. Acad. Sci. **51**, 627 (1949).
[11] R. B. Scheele and M. A. Lauffer, Biochemistry **6**, 3076 (1967).
[12] R. J. Best, Auste. J. Exp. Biol. Med. Sci. **18**, 307 (1940).
[13] J. D. Bernal and I. Fankuchen, J. Gen. Physiol. **25**, 111 (1941).
[14] S. Fraden, A. J. Hurd, M. Cahoon, D. L. D. Caspar, and R. B. Meyer, J. Phys. (Paris) C3, **46**, C3-85 (1985).
[15] F. Lonberg, S. Fraden, A. J. Hurd, and R.B. Meyer, Phys. Rev. Lett. **52**, 1903 (1984).
[16] A. J. Hurd, S. Fraden, F. Lonberg, and R. B. Meyer, J. Phys. (Paris) **46**, 905 (1985).
[17] R. Oldenbourg, X. Wen, R. B. Meyer, and D. L. D. Caspar, Phys. Rev. Lett. **61**, 1851 (1988).
[18] J. A. N. Zasadzinski and R. B. Meyer, Phys. Rev. Lett. **56**, 636 (1986); J. A. N. Zasadzinski, M. J. Sammon, R. B. Meyer, M. Cahoon, and D. L. D. Caspar, Mol. Cryst. Liq. Cryst. **138**, 211 (1986).
[19] M. H. F. Wilkins, Nature (London) **166**, 127 (1950).
[20] J. H. M. Willison, J. Ultrastruct. Res. **54**, 176 (1976).
[21] S. Fraden, D. L. D. Caspar, and W. Phillips, Biophys. J. **37**, 97a (1982).
[22] R. B. Meyer, in *Dynamics and Patterns in Complex Fluids,* edited by A. Onuki and K. Kowasaki, Springer Proceedings in Physics Vol. 52 (Springer-Verlag, Berlin, 1990), p. 62.
[23] G. J. Vroege and H. N. W. Lekkerkerker, Rep. Prog. Phys. **55**, 1241 (1992).
[24] P. Photinos, C. Rosenblatt, T. M. Schuster, and A. Saupe,

J. Chem. Phys. **87**, 6740 (1987).
[25] T. W. Stinson III and J. D. Litster, Phys. Rev. Lett. **25**, 503 (1970).
[26] W. Maier and A. Saupe, Z. Naturforsch. Teil A **15**, 287 (1960).
[27] P. G. de Gennes, Mol. Cryst. Liq. Cryst. **12**, 193 (1971).
[28] J. P. Straley, Mol. Cryst. Liq. Cryst. **22**, 333 (1973).
[29] H. Nakamura and K. Okano, Phys. Rev. Lett. **50**, 186 (1983).
[30] P. G. de Gennes, P. Pincus, and R. M. Velasco, J. Phys. (Paris) **37**, 1461 (1976).
[31] J. P. Straley, Mol. Cryst. Liq. Cryst. **24**, 7 (1973).
[32] P. Photinos and A. Saupe, Mol. Cryst. Liq. Cryst. **123**, 217 (1985).
[33] T. Sato and A. Teramoto, Physica A **176**, 72 (1991).
[34] S. D. Lee, J. Chem. Phys. **87**, 4972 (1987).
[35] A. Stroobants, H. N. W. Lekkerkerker, and Th. Odijk, Macromolecules **19**, 2232 (1986).
[36] Th. Odijk, Macromolecules **19**, 2313 (1986).
[37] J. R. Philip and R. A. Wooding, J. Chem. Phys. **52**, 953 (1970).
[38] R. F. Kayser, Jr., and H. J. Raveché, Phys. Rev. A **17**, 2067 (1977).
[39] H. N. W. Lekkerkerker, Ph. Coulon, R. Van Der Haeger, and R. Deblieck, J. Chem. Phys. **80**, 3427 (1984); Th. Odijk and H. N. W. Lekkerkerker, *ibid.* **89**, 2090 (1985).
[40] P. A. Monson and M. Rigby, Mol. Phys. **35**, 1337 (1978).
[41] D. Frenkel, J. Phys. Chem. **92**, 3280 (1988).
[42] S. D. Lee, J. Chem. Phys. **89**, 7036 (1988).
[43] A. M. Somoza and P. Tarazona, Phys. Rev. Lett. **61**, 2566 (1988).
[44] M. H. V. Van Regenmortel, in *Handbook of Plant Virus Infections and Comparative Diagnosis,* edited by E. Kurstak (North-Holland, Amsterdam, 1981), Chap. 19, pp. 541–564.
[45] A. Klug and D. L. D. Caspar, Adv. Virus Res. **7**, 225 (1960).
[46] H. Boedtker and N. S. Simmons, J. Am. Chem. Soc. **80**, 2550 (1958).
[47] G. Maret and G. Weill, Biopolymers **22**, 2727 (1983).
[48] S. L. Brenner and D. A. McQuarrie, Biophys. J. **13**, 301 (1973).
[49] B. M. Millman, T. C. Irving, B. G. Nickel, and M. E. Loosley-Millman, Biophys. J. **45**, 551 (1984).
[50] J. C. Maxwell, *Treatise on Electricity and Magnetism* (Oxford University Press, New York, 1873), 2 volumes; J. A. Stratton, *Electro Magnetic Theory* (McGraw-Hill, New York, 1941), Sec. 3.27.
[51] M. A. Lauffer, J. Phys. Chem. **42**, 935 (1938).
[52] R. E. Franklin, Biochem. Biophys. Acta **18**, 313 (1955).
[53] C. T. O'Konski, K. Yoshioka, and W. H. Orttung, J. Amer. Chem. Soc. **63**, 1558 (1959).
[54] E. Loh, E. Ralston, and V. N. Schumaker, Biopolymers **18**, 2549 (1979); E. Loh, **18**, 2569 (1979).
[55] S. Fujime and M. Maruyama, Macromolecules **6**, 237 (1973).
[56] P. W. Neurath, in *Biological Effects of Magnetic Fields,* edited by M. F. Barnothy (Plenum Press, New York, 1964), Chap. 2.
[57] Landolt-Börnstein, *Numerical data and functional relationships in science and technology,* New Series, Group II-Vol. 16, edited by O. Madelung, (Springer-Verlag, Berlin, 1986). p. 227 and 296.
[58] D. L. D. Caspar, Adv. Protein Chem. **18**, 37 (1963).
[59] J. Torbet and G. Maret, Biopolymers **20**, 2657 (1981).
[60] G. Maret and K. Dransfeld, in *Strong and Ultrastrong Magnetic Fields and Their Applications,* edited by F. Herlach, Topics in Applied Physics Vol. 57 (Springer-Verlag, Berlin, 1985), Chap. 4.
[61] P. G. de Gennes, *The Physics of Liquid Crystals* (Clarendon, Oxford, 1975).
[62] D. Frankel (personal communication).
[63] The error resulted from confusing the tabulated values for the packing fraction η, in Table I of Ref. [34], with the scaled packing fraction η^*, of Fig. 1 of Ref. [34].
[64] F. S. Allen and K. E. Van Holde, Biopolymers **10**, 865 (1971).
[65] T. J. Sluckin, Liq. Cryst. **6**, 111 (1989).
[66] K. Kajiware, N. Donkai, Y. Hirage, and H. Inagaki, Makromol. Chem. **187**, 2883 (1986).
[67] For example, H. K. Schachman,, *Ultracentrifugation in Biochemistry* (Academic, New York, 1959).
[68] J. Wilcoxon and J. M. Schurr, Biopolymers **22**, 849 (1983).
[69] S. Broersma, J. Chem. Phys. **32**, 1632 (1960); **74**, 6989 (1981).

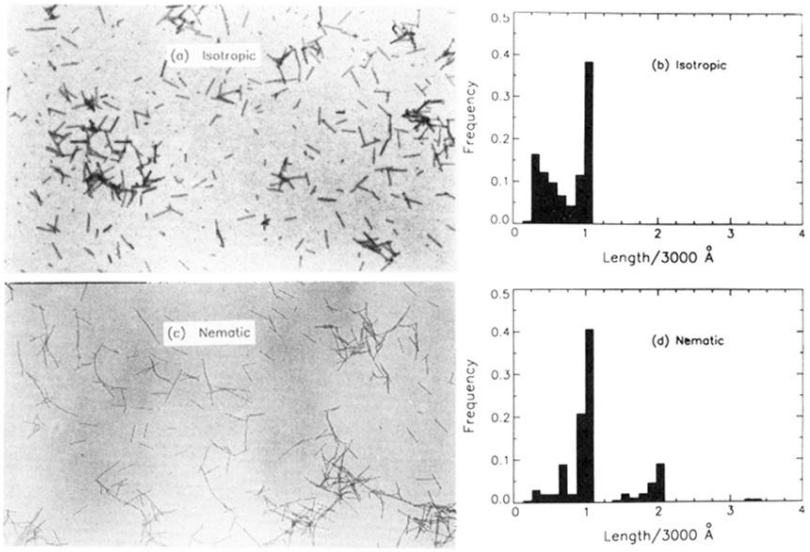

FIG. 11. Electronmicrographs of material taken from each of the coexisting isotropic and nematic phases showed segregation of the longer particles into the nematic phase. The photographs are from the U2 5 m*M* fragmented sample of Fig. 10. (a) Isotropic phase, (b) length histogram obtained from (a) in units of the monomer length (3000 Å), (c) nematic phase, and (d) length histogram of (c).